PHILOSOPHICAL TRANSACTIONS OF THE ROYAL SOCIETY A MATHEMATICAL, PHYSICAL & ENGINEERING SCIENCES

The Excitation of Surface Waves near a Cut-Off Frequency

B.J.S. Barnard, J.J. Mahony and W.G. Pritchard

Phil. Trans. R. Soc. Lond. A 1977 **286**, 87-123
doi: 10.1098/rsta.1977.0111

THE EXCITATION OF SURFACE WAVES NEAR A CUT-OFF FREQUENCY

By B. J. S. BARNARD, J. J. MAHONY† and W. G. PRITCHARD
Fluid Mechanics Research Institute, University of Essex, Colchester

(*Communicated by T. B. Benjamin, F.R.S. – Received* 17 *September* 1976)

CONTENTS

PAGE

1. Introduction 88
2. Derivation of the nonlinear equations 91
   - 2.1. Formulation of the problem 91
     - 2.1.1. The driving condition at the wavemaker 91
   - 2.2. A theory for the inviscid nonlinear response 94
   - 2.3. A theory for dissipative effects 96
3. The response near the cut-off frequency 98
   - 3.1. Inviscid linear theory 98
   - 3.2. Viscous linear theory 98
   - 3.3. Nonlinear theory 99
     - 3.3.1. Inviscid model 99
     - 3.3.2. Dissipative model 103
     - 3.3.3. Numerical solutions 104
4. Experimental apparatus 107
5. Experimental results 108
   - 5.1. The response at a given X 109
   - 5.2. The phase at $X = 0$ 111
   - 5.3. The structure along the channel 112
   - 5.4. The response as a function of depth 115
   - 5.5. The structure across the channel 116
   - 5.6. Conclusion 116

Appendix A. A catalogue of failures 120

Appendix B. The magnitude of the dissipative effects 122

References 123

This paper describes a study of surface waves in a uniform channel, where the waves are generated by a plane flap executing torsional oscillations about a vertical axis at a frequency near a cut-off value for a wave mode. Experiments indicate that, near a cut-off frequency, the wave response is relatively large, and indeed linear inviscid theory suggests that the wave amplitudes are infinitely large at the cut-off frequency itself.

† Permanent address: Department of Mathematics, University of Western Australia, Nedlands, Western Australia.

Vol. 286. A 1333. 12 [Published 20 June 1977

Here we present theories for the modification of this result by making allowance (separately) for nonlinear terms in the surface boundary condition and for viscous dissipation. In order to estimate the effectiveness of the wavemaker in forcing the motions, a separate calculation was made to apportion the driving condition into a part driving a parasitic non-propagating field and a part forcing the wave modes.

Also described in the paper are experiments in which the wave response has been measured in a similar situation to that modelled by the analytic work, and one of the main purposes of this study is to try to ascertain how well the theoretical model describes the experimental situation. An important feature to emerge from the comparison is that, even though the observed wave amplitudes were rather large and the temporal decay rate of standing waves corresponding to the cut-off mode was quite small, the dissipative effect played a crucial rôle in determining the structure of the response. Because of this the theoretical response was determined by numerical computation. Some of the results show a similarity with the response of a nonlinear spring, but there are significant differences.

The results indicate that the model gave a good qualitative description of the experiments, and accordingly our main conclusions to the study are:

(i) the multiple-scale calculation, by which the nonlinear effects were estimated, appears to have given useful results in this particular case;

(ii) the way in which the dissipative effects were modelled appears to have been satisfactory;

(iii) the method of estimating the effective driving condition at the wavemaker seems to have worked very well.

1. Introduction

In a paper on resonant phenomena of surface waves on a beach, Ursell (1952) compared the predictions of a linear surface-wave theory with laboratory measurements. His experiments were made in a water channel with a beach at one end, and surface waves (antisymmetric about the axis of the channel) were excited by an appropriate periodic motion of false side walls at the beach section. Ursell's analysis, based on a linearized surface-wave theory of the natural modes of the system, yields a discrete spectrum of Stokes' edge waves together with a set of continuous spectra (each with its own cut-off) for the antisymmetric modes propagating along the channel. For forced motions, as in the experiments, the theory predicts large responses for excitation frequencies close to those of the discrete edge waves and also at frequencies close to the cut-off frequencies. The large response near the cut-off frequency can be explained physically by noting that the group velocity along the channel becomes vanishingly small as the cut-off frequency is approached (from above), and thus the energy fed into such a mode does not radiate away from the wavemaker. In his experiments Ursell was concerned mainly with the variation of the surface response as a function of the excitation frequency, and the results confirm the general qualitative features of the linearized theory, although there is some indication of a small frequency shift for the maximum amplitude of response.

A strict comparison between the theory and the experiment is not possible since the theory predicts infinite wave amplitudes at the natural edge-wave and cut-off frequencies, and Ursell observed that either, or both, nonlinear and dissipative effects must be important in determining the actual forced response for the 'resonant' conditions. Ursell gave a partial theory, based on dissipative effects in the side-wall boundary layers, but had to guess the value of the decay rate near a cut-off frequency. At the time this investigation was begun no better discussion of the factors determining the forced resonant response had been given. The initial attempts to determine an appropriate theoretical model were described in a report by Mahony (1971), but it was

evident from the initial laboratory experiments that the theory was not able to describe all the major features of the observations. Subsequently the theory was applied by Ockendon & Ockendon (1973) in an attempt to describe the response near the cut-off frequency in terms of soft and hard springs.

This paper is concerned with methods of determining such fields theoretically when allowance is made both for nonlinear and dissipative effects. In situations involving nonlinear wave propagation the calculations can, at present, only be carried out by concentrating on what are thought to be the significant terms, and the validity of answers obtained by using such procedures must be considered seriously. Theoretical methods of this kind have recently been used on a number of occasions (see, for example, Cole 1968; Nayfeh 1973) but there is little concrete experimental evidence to indicate the accuracy or qualitative usefulness of their predictions; accordingly we have tried, in this study, to model a physical situation in which a close comparison can be made with experimental observations. Unfortunately Ursell's experimental results are not suitable for such a comparison since the measurements were made at a fixed amplitude of excitation (with the result that it is difficult to distinguish the nonlinear effects from the dissipative effects), and no results are given of the variation of the wave amplitudes along the channel. Thus it was decided to carry out a new set of experiments to check the theoretical methods adopted in this work and, in order to simplify both the theoretical calculations and the experimental apparatus, we have worked with a simpler geometric configuration than that used by Ursell.

The arrangement considered here is that of an open channel of uniform depth in which the antisymmetric modes are generated by a wavemaker operating at one end. A simple practical wavemaker is a vertical plate performing small rotational oscillations about a vertical axis through the centre of the channel. Such a wavemaker can generate many transverse wave modes (as well as parasitic, localized, modes which do not propagate down the channel) and the aim of the calculations is to predict the response when the wavemaker is driven at a frequency close to a natural-mode cut-off frequency.

The initial part of the paper attempts to assess the effectiveness of such a wavemaker in generating the wave field. This has been done by partitioning the wavemaker action into one driving a strictly localized, non-resonant, field (the parasitic field) and one driving the resonant, modal, wave field. (Such a procedure corresponds to a decomposition into a complete set of eigenfunctions as described by Havelock 1929). The latter of these is then used as a forcing effect driving the natural modes in the channel. A heuristic theory is then developed for the nonlinear response of such waves when driven at a frequency close to the lowest natural-mode cut-off frequency. But it is possible that the unbounded motions predicted by the linear theory at the cut-off frequency are limited by dissipative effects rather than nonlinearities of the wavefield, and accordingly a separate (linear) theory has been developed to account for a small amount of dissipation at the walls of the channel. However, theoretical estimates of the damping of water waves usually prove to be inaccurate, and therefore the theory has been developed to determine the way in which the dissipative effect should be included in the model rather than trying to estimate its actual magnitude. The idea is that the appropriate coefficients in the model equation should be determined empirically from observations on the rate of decay of a related mode excited in the channel. Since both the nonlinear and the dissipative effects are calculated independently as small corrections to the basic linear system, a composite model equation is formed by including both modifications additively on the assumption that the coupling between them is negligibly small.

Having derived, in § 2, theoretical models for the wave motions, we describe in § 3 some of the

PHILOSOPHICAL TRANSACTIONS OF THE ROYAL SOCIETY A MATHEMATICAL, PHYSICAL & ENGINEERING SCIENCES

motions that might be realized in the channel. Our initial expectations had been, like Ockendon & Ockendon (1973), that nonlinear effects would predominate over dissipative effects and this seemed to be confirmed by measurements of the wave amplitudes near the wavemaker as a function of frequency. In fact, if we had been content to use this comparison as the only criterion for determining the validity of the theory we would have been able to report rather good agreement between the theory and the experiments: the hard and soft spring ideas discussed by the Ockendons would have appeared to give a good description of the experimental situation. However, further observations on the phase and on the wave amplitude along the channel (together with the observation that the response was rather small when the nonlinear coefficient was small) were not as described by these theories, and it eventually became apparent to us that the dissipative effects were playing a crucial rôle in determining the structure of the wave motions, despite the fact that the decay time of the waves was some hundreds of periods of the motion. (A brief outline is given in appendix A of the experimental and theoretical considerations leading to this situation.)

The physical reason why the dissipative effects can sometimes play an important rôle is as follows. Suppose that the nonlinear terms were the only ones to prevail. Then, the steady state that would be approached, requires the radiation of energy to infinity by the wave field: at frequencies below the cut-off value this can occur only if the wave amplitude is large enough. But the presence of only a small amount of dissipation results in a decaying wave field which cannot accept the energy flux implied by the inviscid limit. Thus, there are parameter ranges for which small dissipative effects are important, when it might be expected, on crude order-of-magnitude arguments, that they would be of only minor significance. Accordingly, the phase of the waves, which is closely associated with the rate at which energy is transferred from the paddle into the wave field, is a much more significant test of the physics than the more obvious variable, the wave amplitude near the paddle.

With the inclusion of the dissipative effects we were unable to obtain analytic solutions to the model equations, and so a method was devised by means of which numerical solutions could be found. It was the very good overall agreement of these solutions with the experimental observations that suggested to us the following major conclusions to our studies.

(i) The method of assessing the effectiveness of the wavemaker in generating the wave field appears to have been very successful. There is no direct way of checking the success of this calculation, but we feel that the very good overall agreement between the observed and the predicted wave amplitudes lends considerable support to its usefulness.

(ii) It appears from the results that the modelling of the nonlinear effects was fairly successful. This suggests, for the present case, that the heuristic methods used to estimate the important nonlinear terms have provided a very useful description of the experimental situation.

(iii) Although we have not attempted to give a quantitative description of the dissipative effects, the results suggest that the way dissipation influences the motions is represented fairly well by the inclusion in the model equation of a linearly additive damping term of the kind described in § 2.

PHILOSOPHICAL TRANSACTIONS OF THE ROYAL SOCIETY A MATHEMATICAL, PHYSICAL & ENGINEERING SCIENCES

2. Derivation of the nonlinear equations

2.1. *Formulation of the problem*

Consider the irrotational motion of an inviscid fluid in a channel of width b and filled to a depth d. We suppose that the motions are generated by periodic oscillations of a wavemaker at one end of the channel. Let $Oxyz$ be rectangular cartesian axes with the x-axis along the channel and the z-axis vertically upwards. The origin is taken to be on one wall of the channel at the point defined by the undisturbed position of the wavemaker and the free surface. Let the coordinates of an arbitrary point relative to these axes be (bx, by, bz) and choose the unit of time to be $(b/g)^{\frac{1}{2}}$, where g is the acceleration due to gravity. All other kinematic units are formed by appropriate combinations of b with the unit of time. In particular, let the velocity potential at time $(b/g)^{\frac{1}{2}}t$ be $(b^3/g)^{\frac{1}{2}}\phi(x, y, z, t)$ and the surface displacement be $b\zeta(x, y, t)$. The velocity potential satisfies Laplace's equation

$$\nabla^2\phi = 0, \tag{2.1}$$

together with the following boundary conditions:

(i) at the free surface (assuming that surface tension may be neglected)

$$\left.\begin{aligned} \phi_z &= \zeta_t + \phi_x\zeta_x + \phi_y\zeta_y, \\ \phi_t + \zeta + \tfrac{1}{2}(\phi_x^2 + \phi_y^2 + \phi_z^2) &= 0; \end{aligned}\right\} \tag{2.2}$$

(ii) on the rigid boundaries of the channel

$$\left.\begin{aligned} \phi_y &= 0 \quad \text{on} \quad y = 0, 1, \\ \phi_z &= 0 \quad \text{on} \quad z = -\beta, \end{aligned}\right\} \tag{2.3a, b}$$

where $\beta = d/b$;

(iii) the conditions at the wavemaker. The specification of this is discussed below;

(iv) the condition at the end of the channel opposite the wavemaker. Theoretically it is desirable to consider an open-ended channel, in which case it would be necessary to formulate a suitable radiation condition; in the experiments we try to simulate this condition by absorbing the waves on a beach. Thus there is a certain difficulty in choosing the appropriate radiation condition and accordingly we shall, for the present, leave this condition free.

2.1.1. *The driving condition at the wavemaker*

The simplest practical wavemaker able to generate waves in a cut-off mode appears to be a stiff flat plate, centrally hinged, and undergoing angular rotations of small amplitude θ about a vertical axis through the centre of the channel. Let Ω be the angular frequency of this motion and write $\omega = \Omega(b/g)^{\frac{1}{2}}$. Then the appropriate boundary condition on the wavemaker is

$$\frac{\mathrm{D}}{\mathrm{D}t}\{x\cos(\theta\sin\omega t) + (y - \tfrac{1}{2})\sin(\theta\sin\omega t)\} = 0.$$

If we now consider an approximation to this equation, made on the basis that both θ and ϕ are small, we find at the wavemaker that

$$\phi_x(0, y, z, t) = -\omega\theta(y - \tfrac{1}{2})\cos\omega t + O(\theta\phi) \tag{2.4a}$$

which may also be expressed in terms of its Fourier representation by

$$\phi_x(0, y, z, t) \approx 4\omega\theta\pi^{-2} \sum_{n=0}^{\infty} (2n+1)^{-2} \cos[(2n+1)\,\pi y] \cos \omega t. \tag{2.4b}$$

The natural antisymmetric modes of the channel are easily found when the linear form of the free-surface condition is used (cf. Ursell 1952), and they take the form

$$\left.\begin{aligned} \phi &\sim \cosh \kappa(z+\beta) \cos[(2n+1)\,\pi y]\, \mathrm{e}^{\pm \mathrm{i}\omega t}\, \mathrm{e}^{\pm kx}, \\ \text{where} \quad \omega^2 &= \kappa \tanh \kappa\beta \\ \text{and} \quad k^2 &= (2n+1)^2\,\pi^2 - \kappa^2. \end{aligned}\right\} \tag{2.5}$$

Thus the boundary condition (2.4*b*) at the wavemaker indicates that all the antisymmetric modes will be excited, but it depends on the values of ω and n whether these modes are generated as exponentially-decaying or as wave-structured components. In this study, we shall restrict our attention specifically to the case for which the dimensionless frequency ω of the wavemaker is close to the value γ for which the lowest mode $n = 0$ has $k = 0$, namely

$$\gamma^2 = \pi \tanh \pi\beta. \tag{2.6}$$

Accordingly all the higher modes decay exponentially away from the wavemaker and are not likely to be as strongly excited as the cut-off mode at the frequency γ. (In this respect Ursell's (1952) experiments offer clear evidence that much larger responses occur at frequencies close to those at which a mode becomes a cut-off mode.) When, to this effect, we include the contribution of the factors $(2n+1)^{-2}$, it seems reasonable to make a further approximation to (2.4*b*) and describe the boundary condition at the wavemaker by

$$\phi_x(0, y, z, t) = 4\omega\theta\pi^{-2} \cos \pi y \cos \omega t. \tag{2.7}$$

However, it must be remembered that each Fourier component $\cos(2n+1)\,\pi y$ has associated with it a parasitic non-propagating field. This arises because the excitation of the wavemaker is uniform with depth and therefore does not reflect the variation in z of the natural modes. But there is no reason to suppose that these parasitic fields, which decay very rapidly along the channel, should be strongly excited by the wavemaker. Certainly there is no evidence of this from the experiments.

On the other hand, there is also a parasitic field associated with the cut-off mode. It seems unlikely that we can neglect this parasitic field completely, but to retain it would appear to rule out the possibility of describing the nonlinear surface condition for the cut-off mode. Thus it was decided to arrange the boundary condition on the wavemaker in the form

$$\begin{aligned} \phi_x(0, y, z, t) = {} & 4\omega\theta\pi^{-2} \cos \pi y \cos \omega t \{1 - \sigma \cosh \pi(z+\beta) \operatorname{sech} \pi\beta\} \\ & + 4\omega\theta\pi^{-2}\sigma \cos \pi y \cos \omega t \cosh \pi(z+\beta) \operatorname{sech} \pi\beta, \end{aligned}$$

with a view to choosing σ so that the first term, when used in conjunction with the linearized surface condition, gives rise to a purely parasitic field at the cut-off frequency $\omega = \gamma$. Then, for the discussion of the nonlinear theory of the cut-off mode, the boundary condition at the wavemaker is applied in the form

$$\phi_x(0, y, z, t) = 4\omega\theta\pi^{-2}\sigma \cos \pi y \cos \omega t \cosh \pi(z+\beta) \operatorname{sech} \pi\beta,$$

where σ is determined by the above criterion, and the frequency ω is assumed to be close to γ.

It is virtually impossible to assess how accurate such a partitioning is likely to be and this feature must remain one of the unresolved questions about the theory. This partitioning is equivalent to using a full modal decomposition allowing for the variation with depth, such as has been used by Havelock (1929), but neglecting the other components in the higher-order surface condition. It is typical of most models for nonlinear effects in the theory of water waves.

The determination of the appropriate value of σ is a standard problem in linear analysis: we seek a velocity potential ϕ in the form

$$\phi = \Phi(x, z) \cos \pi y \cos \gamma t,$$

which satisfies the following boundary conditions:

(i) at the free surface

$$\Phi_z(x, 0) = \gamma^2 \Phi(x, 0);$$

(ii) at the bottom of the channel

$$\Phi_z(x, -\beta) = 0;$$

(iii) at the wavemaker

$$\Phi_x(0, z) = 4\omega\theta\pi^{-2}\{1 - \sigma \cosh \pi(z+\beta) \operatorname{sech} \pi\beta\};$$

(iv) the potential $\Phi \to 0$ as $x \to \infty$.

If Φ is extended to the interval $(-\infty, \infty)$ in x by its even continuation, the Fourier transform $\hat{\Phi}(k, z)$ of that continuation satisfies the equation

$$\hat{\Phi}_{zz} - (k^2 + \pi^2)\,\hat{\Phi} = 8\omega\theta\pi^{-2}\{1 - \sigma \cosh \pi(z+\beta) \operatorname{sech} \pi\beta\}$$

and the boundary conditions

$$\hat{\Phi}_z(k, -\beta) = 0, \quad \hat{\Phi}_z(k, 0) = \gamma^2 \hat{\Phi}(k, 0).$$

A routine calculation then shows that

$$\left.\begin{aligned} \hat{\Phi}/(8\omega\theta\pi^{-2}) = {} & -(k^2+\pi^2)^{-1} + \sigma k^{-2} \cosh \pi(z+\beta) \operatorname{sech} \pi\beta \\ & - C \cosh[(k^2+\pi^2)^{\frac{1}{2}}(z+\beta)] \operatorname{sech}[(k^2+\pi^2)^{\frac{1}{2}}\beta], \\ \text{where} \quad C = {} & \gamma^2(k^2+\pi^2)^{-1}\{(k^2+\pi^2)^{\frac{1}{2}} \tanh[(k^2+\pi^2)^{\frac{1}{2}}\beta] - \gamma^2\}^{-1}. \end{aligned}\right\} \tag{2.8}$$

It follows from equation (2.8) that $\hat{\Phi}$ has a double pole at $k = 0$, and accordingly we wish to choose a value of σ to cancel this pole in the equation for $\hat{\Phi}$. Thus, with

$$\sigma = 2\gamma^2\pi^{-1}\{\pi\beta \operatorname{sech}^2 \pi\beta + \tanh \pi\beta\}^{-1},$$

$\hat{\Phi}$ is free of singularities for real values of k so that the corresponding potential ϕ vanishes in the limit of $x \to \infty$. For any other value of σ the corresponding solution ϕ would have outgoing waves at infinity.

Thus, the above arguments suggest that, if we can partition the influence of the wavemaker into two uncoupled parts (namely, one which drives the non-resonant parasitic field and one which supplies the drive for the natural mode), the forcing effect of the wavemaker for the cut-off mode is represented by

$$\left.\begin{aligned} \phi_x(0, y, z, t) = {} & \epsilon \cos \pi y \cosh \pi(z+\beta) \operatorname{sech} \pi\beta \cos \omega t \\ \text{where} \quad \epsilon = {} & 8\theta\gamma^3\pi^{-3}\{\pi\beta \operatorname{sech} \pi\beta + \tanh \pi\beta\}^{-1}. \end{aligned}\right\} \tag{2.9}$$

In this equation ϵ can be interpreted as the driving amplitude of a flexible wavemaker which exactly reproduces the velocity variations (with depth) of the antisymmetric wave mode being generated. This value of ϵ will henceforth be referred to as 'the wavemaker amplitude' and will be used in all the subsequent analysis and in the comparisons with the experiments.

2.2. *A theory for the inviscid nonlinear response*

The form of the forcing effect (2.9) of the wavemaker is identical with that of the natural mode at the frequency $\omega = \gamma$ and accordingly there is no solution to the linearized problem when the wavemaker operates at this frequency. Here we shall assume that it is the nonlinear effects in the surface condition, but not on the wavemaker, which limit the surface response as the cut-off frequency is approached.

First, we must assess the relevant scales for the structure of the motions in the present situation. As the dimensionless driving frequency ω approaches the cut-off frequency γ, the length scale of either the travelling wave or the exponential decay along the channel increases beyond bound if the results of the linearized theory are accepted (cf. equation (2.5)). Here we shall assume that, once nonlinear effects become important, there is some large length scale $L(\epsilon)$ associated with the variations along the channel. Let the order of magnitude of the velocity potential be $\alpha(\epsilon)$, then the boundary condition at the wavemaker implies that α/L is $O(\epsilon)$.

However, another condition is required to determine both α and L, and for this we must rely on heuristic arguments which will mirror the subsequent mathematics. Since L is large the x-derivatives in Laplace's equation are smaller than the other terms and the motion is essentially that of a two-dimensional standing wave across the channel. Accordingly we are led to consider a surface profile of the form

$$\alpha A(L^{-1}x)\cos \pi y \exp(\mathrm{i}\omega t),$$

together with higher-order terms. In problems such as this the only higher-order terms which are of concern are those with the same spatial and temporal variations as the leading term, for it is through them that significant nonlinear effects can enter. For water waves it is well known (see, for example, Tadjbakhsh & Keller 1960) that such terms enter the surface condition at $O(\alpha^3)$ and not earlier in the calculations. Furthermore, the neglected x-derivatives enter the calculations as a term of $O(\alpha L^{-2})$ in Laplace's equation and accordingly affect the calculations in the surface condition at the same order.

Thus, if $\alpha L^{-2} \gg \alpha^3$ we can expect a spatial distribution along the channel of the form predicted from linear theory. If, on the other hand, $\alpha^3 \gg \alpha L^{-2}$ we would expect to recover nonlinear standing waves with relatively unimportant variations along the channel. This suggests, when looking for cases where there is a balance between nonlinear effects and variations along the channel, that α^3 and αL^{-2} are of the same order. Then the two estimates $\alpha L = O(1)$ and $\alpha L^{-1} = O(\epsilon)$ suggest a scaling in which α is $O(\epsilon^{\frac{1}{2}})$ and L is $O(\epsilon^{-\frac{1}{2}})$. An estimate of the bandwidth of frequencies for the nonlinear dominated response can be made on the expectation that the detuning term should not enter the surface condition at an earlier stage than the important nonlinear term. Thus it is assumed that $\omega - \gamma$ is $O(\alpha^2)$ or equivalently $\omega - \gamma$ is $O(\epsilon)$.

These heuristic arguments suggest seeking a solution in the form

$$\left.\begin{aligned}\phi(X,y,z,t) &= \epsilon^{\frac{1}{2}}\phi_0 + \epsilon\phi_1 + \epsilon^{\frac{3}{2}}\phi_2 + \ldots \\ \text{and} \qquad \zeta(X,y,t) &= \epsilon^{\frac{1}{2}}\zeta_0 + \epsilon\zeta_1 + \epsilon^{\frac{3}{2}}\zeta_2 + \ldots,\end{aligned}\right\} \tag{2.10}$$

where

$$X = \epsilon^{\frac{1}{2}}x, \tag{2.11}$$

and introducing a parameter λ (assumed to be unit order at most) such that

$$\omega^2 = \pi \tanh \pi\beta + \lambda\epsilon. \tag{2.12}$$

We now carry out a regular perturbation procedure. The general solution obtained from the first order terms is

$$\phi_0 = \tfrac{1}{2}\{A_0(X)\, e^{i\gamma t} + *\} \cos \pi y \cosh \pi(z+\beta) \operatorname{sech} \pi\beta, \tag{2.13}$$

where $*$ denotes the complex conjugate of the preceding term in the bracket.† In this expression $A_0(X)$ is a complex-valued function which is arbitrary except that the boundary condition on the wavemaker requires that

$$A_0'(0) = 1. \tag{2.14}$$

Usually the procedure now would be to continue the perturbation expansion to successively higher orders. But in the present case it is not necessary to carry out the detailed calculations as the results are already available in the literature from work on standing surface waves. An equation which may be used to determine A_0 is derived from the $O(\epsilon^{\frac{3}{2}})$ terms in the free-surface boundary conditions, but terms involving derivatives of A_0 do not arise in the free-surface condition until $O(\epsilon^2)$ and accordingly, at $O(\epsilon^{\frac{3}{2}})$, A_0 can be treated as a constant. In particular the calculation of the free-surface condition to $O(\epsilon^{\frac{3}{2}})$, in the present case, is identical with the calculation for standing waves and is given by the relation

$$\phi_{2tt} + \phi_{2z} = \{K(A_0)\, e^{i\gamma t} + *\} + \text{non-resonant terms}, \tag{2.15}$$

where we assume that the depth is chosen so that none of the higher harmonics is a natural mode. The term $K(A_0)$ can be deduced from the known results for standing waves, as the condition (2.15) implies that a standing wave cannot have a frequency γ but must oscillate at a frequency σ given by

$$-\tfrac{1}{2}(\sigma^2 - \gamma^2) A_0 = \epsilon K(A_0) + o(\epsilon).$$

This equation merely reflects the usual Poincaré correction for the nonlinear dependence of frequency; the actual correction is given by Tadjbakhsh & Keller (1960), from which we have (after a minor calculation to allow for differences in notation) that

$$\left.\begin{aligned} K(A_0) &= \tfrac{1}{2} D(A_0^2 A_0^* + *), \\ \text{where} \qquad D &= -\tfrac{1}{32}\pi^4(9\coth^6 \pi\beta - 12\coth^2 \pi\beta - 3\tanh^2 \pi\beta - 2\tanh^6 \pi\beta). \end{aligned}\right\} \tag{2.16}$$

Having obtained the results of the calculations of the nonlinear surface condition we turn to the problem of determining the function ϕ_2. It satisfies the partial differential equation

$$\phi_{2yy} + \phi_{2zz} = -\{A_0''(X)\, e^{i\gamma t} + *\} \cosh \pi(z+\beta) \operatorname{sech} \pi\beta,$$

together with the boundary conditions

$$\phi_{2y} = 0 \quad \text{on} \quad y = 0, 1,$$

$$\phi_{2z} = 0 \quad \text{on} \quad z = -\beta,$$

and

$$\phi_{2tt} - \phi_{2z} = \lambda\phi_0 + \tfrac{1}{2} D(A_0^2 A_0^*\, e^{i\gamma t} + *) \cos \pi y.$$

We look for a solution for ϕ_2 in the form

$$Z(z)\{A_2(X) + *\} \cos \pi y \operatorname{sech} \pi\beta,$$

† The complex form has been adopted here because it is not valid in general to assume that the field is in phase with the wavemaker.

and in order to ensure that a solution exists to the resulting Sturm–Liouville problem for Z it is necessary that an orthogonality condition is satisfied. Such a calculation yields the consistency condition

$$aA_0'' + \lambda A_0 + DA_0^2 A_0^* = 0, \tag{2.17}$$

where

$$a = (4\pi)^{-1} \operatorname{sech}^2 \pi\beta (2\pi\beta + \sinh 2\pi\beta).$$

This equation, together with the boundary condition (2.14) and some appropriate boundary condition far from the wavemaker, provides the means of determining the spatial variation of the wave field along the channel.

2.3. *A theory for dissipative effects*

So far we have assumed that no dissipative mechanisms are present, but it is not possible to decide *a priori* whether the response is controlled by nonlinear or by dissipative effects. It is, unfortunately, very difficult to make accurate theoretical estimates of attenuation factors for water waves in channels because the experimental situation is strongly affected by surface impurities and by wetting effects on the walls. Therefore it was decided to use the experimentally determined lapse (or decay) rate of waves in the channel in order to determine the scale of the dissipative mechanisms; but the way in which the dissipative effects are to be fitted into the mathematical model is based on the action of viscosity. Ursell (1952) made an estimate of the attenuation of various propagating modes but his analysis was applicable only at frequencies sufficiently remote from the cut-off frequency, and there appears to be no estimate available in the literature for the scale of the attenuation near the cut-off frequency. However, such estimates can be obtained using the method of matched asymptotic expansions. Here we shall consider only the case $(\omega^2 - \gamma^2)$ small, for otherwise Ursell's results are applicable.

The key to the present analysis is the calculation of the boundary conditions to the potential flow which would make allowance for the presence of the boundary layers on the walls of the channel. For small-amplitude waves the convective terms in the boundary-layer equations are small, and so the boundary-layer equations are approximately linear. Thus it is possible to calculate a displacement-thickness correction without knowing the details of the potential flow.

To illustrate the calculations, consider the x-component, u, of the flow velocity in the neighbourhood of the wall $y = 0$. It satisfies the equation

$$u_t = \mu^2 u_{yy}, \tag{2.18}$$

where $\mu^2 = \nu(b^3 g)^{-\frac{1}{2}}$ is the reciprocal of the Reynolds number. In practice μ is very small ($\mu \approx 10^{-3}$ in the experiments) and so the boundary-layer equations are well justified.

When the outer flow is sinusoidal, with period ω, equation (2.18) can be solved and we find that the x-component of the velocity field, near $y = 0$, is

$$u = \phi_x(x, y, z)\, e^{i\omega t} - \phi_x(x, 0, z)\, e^{i\omega t} \exp[-(i\omega)^{\frac{1}{2}} \mu^{-1} y],$$

where $i^{\frac{1}{2}}$ has been used for $\exp(\frac{1}{4}i\pi)$. A similar result is obtained for w, the velocity component in the z-direction, and using these two results we can deduce, from the continuity equation, the velocity component in the y-direction. Accordingly, it follows that the appropriate boundary condition for the outer (potential) flow is

$$\phi_y(x, 0, z, t) = \mu(\phi_{xx} + \phi_{zz})/(i\gamma)^{\frac{1}{2}},$$

where γ now replaces ω since the term on the right-hand side is already small.

Thus the viscous linear problem can be described by wave modes which satisfy the partial differential equation

$$\nabla^2\phi = 0$$

and the boundary conditions

$$\left.\begin{aligned} \phi_y &= \Delta(\phi_{xx}+\phi_{zz}) && \text{on} \quad y = 0,\\ \phi_y &= \Delta(\phi_{xx}+\phi_{zz}) && \text{on} \quad y = 1,\\ \phi_z &= \Delta(\phi_{xx}+\phi_{yy}) && \text{on} \quad z = -\beta,\\ \phi_z &= \omega^2\phi && \text{on} \quad z = 0. \end{aligned}\right\} \tag{2.19}$$

For convenience, we have extracted a factor $e^{-i\omega t}$ from the first three boundary conditions; $\Delta = \mu/(i\omega)^{\frac{1}{2}}$.

A solution to (2.19) is now sought in the form

$$\phi = e^{ikx}Y(y)\,Z(z),$$

and we shall restrict our attention to the case in which k is small. Let the functions Y and Z satisfy the equations

$$Y'' = -l^2Y, \quad Z'' = m^2Z,$$

as a result of which the boundary conditions, for small k, are given approximately by

$$\begin{aligned} Y'(0) &= \Delta m^2 Y(0), \quad & Y'(1) &= -\Delta m^2 Y(1),\\ Z'(0) &= \omega^2 Z(0), & Z'(1) &= -\Delta l^2 Z(-\beta). \end{aligned}$$

Thus it follows that the eigenvalues of (2.19) are given approximately by

$$l = \pi(1+2\Delta) + O(\Delta^2)$$

and

$$m = \pi + C_1\Delta + C_2(\omega^2-\gamma^2) + O(\Delta^2, (\omega^2-\gamma^2)^2),$$

where

$$C_1 = 2\pi(1-\tanh\pi\beta)\,|1-e^{-2\pi\beta}-\pi\beta(1-\tanh\pi\beta)|^{-1},$$

and

$$C_2 = |\tanh\pi\beta + \pi\beta\,\mathrm{sech}^2\,\pi\beta|^{-1}.$$

Then, since ϕ satisfies Laplace's equation, we have that $k^2 = m^2 - l^2$ and it follows that

$$k^2 = -2\pi(2\pi - C_1)\,\Delta + 2\pi C_2(\omega^2-\gamma^2) + O(\Delta^2, (\omega^2-\gamma^2)^2). \tag{2.20}$$

Since Δ is complex, the relation (2.20) gives a bounded response for the linear problem when the forcing effect of the wavemaker is of the form indicated in equation (2.9). The order of magnitude of the response is $\epsilon/|k|$, and the length scale along the channel, at the frequency of maximum response, is $O(|2\pi(2\pi - C_1)\,\Delta|^{-\frac{1}{2}})$. It should be noted that these coefficients are fairly sensitive to the depth: for relatively large values of β, C_1 is small, while for small values of β, $C_1 \sim 2\pi\beta^{-1}$; in particular, there is a depth for which higher approximations must be sought and the attenuation rate is much smaller. But the striking feature of the result (2.20) is the implication that the attenuation rate is $O(\mathrm{Re}^{-\frac{1}{4}})$ and not $O(\mathrm{Re}^{-\frac{1}{2}})$ as suggested by Ursell's analysis for frequencies well away from the cut-off frequency γ. The essential difference between his analysis and the present one is that no prior assumptions have been made about the relevant x-scale of the motions.

The form of equation (2.20) suggests an empirical method for estimating the dissipative effects near the cut-off frequency. It is proposed that (2.20) should be replaced by

$$k^2 = C_3 + iC_4 + a^{-1}(\omega^2-\gamma^2), \tag{2.21}$$

PHILOSOPHICAL TRANSACTIONS OF THE ROYAL SOCIETY A MATHEMATICAL, PHYSICAL & ENGINEERING SCIENCES

where C_3 and C_4 are to be inferred from experimental observations on standing waves with $k = 0$. Thus, if we were to establish a standing wave in the channel, with crests parallel to the axis of the channel and with no spatial variation along the channel, measurements of the frequency of this wave and of its temporal decay rate could be used to determine the constants C_3 and C_4.

The nonlinear equation (2.17) for the spatial variation of the wave field along the channel can now be modified so that, in the limit of vanishingly small amplitudes, we obtain the result (2.21). It follows that the generalization of (2.17) is

$$aA_0'' + \{\lambda + \epsilon^{-1} a(C_3 + \mathrm{i}C_4)\} A_0 + DA_0^2 A_0^* = 0,$$

which, with the obvious redefinitions, we shall write as

$$A_0'' + (p + \mathrm{i}q + rA_0 A_0^*) A_0 = 0. \tag{2.22}$$

Then p is a measure of the difference in frequency from that of the natural mode (corrected for attenuation) with $k = 0$; q is a measure of the dissipative effects. This equation will now be used as a basis for estimating the response near the lowest cut-off frequency. It is clear that similar equations could be developed near the cut-off frequencies of higher modes.

3. The response near the cut-off frequency

3.1. *Inviscid linear theory*

The form of the natural antisymmetric modes of the channel, for the linear version of the surface condition, is given in (2.5). Considering only the lowest mode, we may write the velocity potential as

$$\phi = \mathrm{Re}\{(Ge^{kx} + He^{-kx})\, e^{\mathrm{i}\omega t}\} \cos \pi y \cosh \kappa(z + \beta) \operatorname{sech} \kappa\beta, \tag{3.1}$$

where $\omega^2 = \kappa \tanh \kappa\beta$ and $k^2 = \pi^2 - \kappa^2$; G and H are constants which are determined by the amplitude, ϵ, of the wavemaker drive, and a radiation condition at the open end of the channel. Below the cut-off frequency ($\kappa < \pi$) the constant G must vanish in order that ϕ remains bounded at large distances from the wavemaker. Above the cut-off frequency we impose a radiation condition of outward travelling waves, with the result that G is again chosen to be zero. It then follows, for a wavemaker action of the form indicated in (2.9), that the *amplitude* of the wave motion at the surface is given by

$$\left.\begin{aligned} \zeta &= (\gamma\epsilon \cos \pi y/|k|)\, e^{-|k|x}, && \kappa < \pi, \\ \zeta &= \gamma\epsilon \cos \pi y/|k|, && \kappa > \pi. \end{aligned}\right\} \tag{3.2}\dagger$$

This is a particularly easy quantity to measure experimentally. It should also be noted that the amplitudes become indefinitely large as the cut-off frequency is approached.

A sketch showing the amplitude of these waves at $X = 0$ is given in figure 1.

3.2. *Viscous linear theory*

In order to evaluate the viscous linear theory we must, first of all, determine the constants C_3 and C_4 of (2.21). Consider a standing wave in the channel with $k = 0$, and let its observed frequency be σ and the rate-of-decay of its amplitude be δ. It then follows from (2.21) that

$$aC_3 = \gamma^2 - \sigma^2 + \delta^2,$$

and

$$aC_4 = -2\sigma\delta.$$

† In terms of the variables used in (2.22) the linear inviscid solution (3.2), obtained by putting $q = 0, r = 0$ in (2.22), is

$$A_0(X) = \begin{cases} (-p)^{-\frac{1}{4}} \exp[-(-p)^{\frac{1}{2}} X + \mathrm{i}\pi], & p < 0 \\ p^{-\frac{1}{4}} \exp[-\mathrm{i}(p^{\frac{1}{2}} X - \tfrac{1}{2}\pi)], & p > 0. \end{cases}$$

Thus, the linear viscous theory is described by (2.22) with $r \equiv 0$, and $p = \epsilon^{-1}(\omega^2 - \sigma^2 + \delta^2)$, $q = \epsilon^{-1}(2\sigma\delta)$. The solution satisfying the boundary condition (2.14) and which is bounded as $X \to \infty$ is given by

$$A_0(X) = h \exp\{-(K_1 + iK_2) X\}, \tag{3.3}$$

where $$h = (-K_1 + iK_2)/(K_1^2 + K_2^2),$$

and $$K_1 = \{\tfrac{1}{2}[-p + \sqrt{(p^2 + q^2)}]\}^{\frac{1}{2}},$$

$$K_2 = -q\{2[-p + \sqrt{(p^2 + q^2)}]\}^{-\frac{1}{2}}.$$

A sketch of the response $|A_0(0)| = (K_1^2 + K_2^2)^{-\frac{1}{2}}$ is given in figure 1 for $q = 1, 5, 10$.

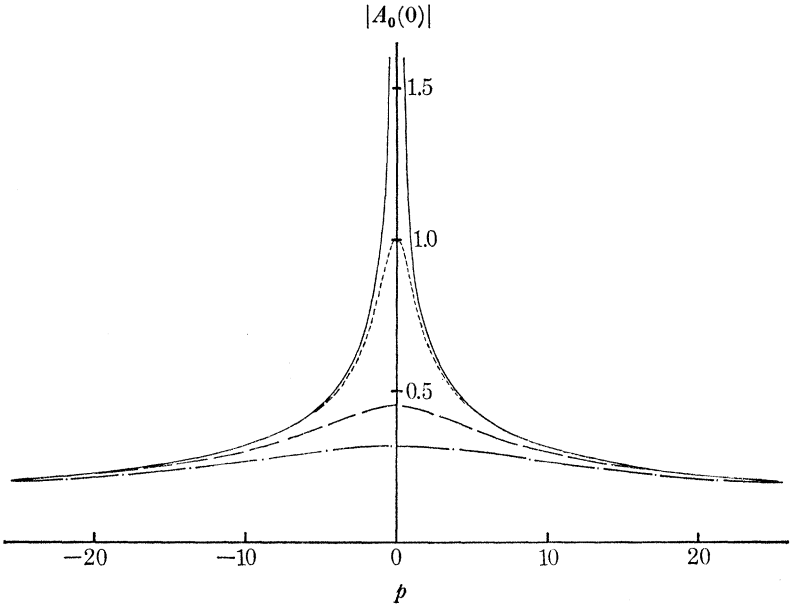

FIGURE 1. The amplitude response $|A_0(0)|$ according to the linear theories. ——, Inviscid theory (equation 3.2); - - - - -, viscous theory, $q = 1.0$ (equation 3.3); — —, viscous theory, $q = 5.0$ (equation 3.3); —·—, viscous theory, $q = 10.0$ (equation 3.3).

3.3. *Nonlinear theory*

Preliminary observations of the decay time, several hundred periods, of the related mode (with $k = 0$) suggested to us that nonlinear effects were likely to be more important than dissipation in determining the cut-off response in our experiments. Moreover, this impression was strengthened by the observation that the response was much larger at frequencies below the cut-off point than above it, in contrast to what is expected if dissipation is the dominant effect (cf. 3.3). Thus, since the experiments were to be made in a channel of only moderate length, we decided to use the inviscid model as a starting point for the theoretical discussion.

3.3.1. *Inviscid model*

When dissipative effects are neglected the resulting equation for the variation of the wave amplitude along the channel is

$$A_0'' + (p + rA_0 A_0^*) A_0 = 0. \tag{3.4}$$

This equation can be simplified by the introduction of new (real-valued) functions R, ψ representing the amplitude and phase of the waves. Thus, we have that

$$A_0(X) = R(X)\,e^{i\psi(X)}.$$

Using this substitution, and separating real and imaginary parts of (3.4) we find that

$$R'' - R\psi'^2 + pR + rR^3 = 0, \tag{3.5}$$

and

$$2R'\psi' + R\psi'' = 0.$$

The latter of these equations can be integrated immediately to give

$$R^2\psi' = M, \tag{3.6}$$

where M is a constant. Then, using (3.6) to eliminate ψ' from (3.5), we can form an energy integral from the resulting equation to give

$$R'^2 + M^2R^{-2} + pR^2 + \tfrac{1}{2}rR^4 = N, \tag{3.7}$$

where N is another constant. Thus (3.7) is an equation for the wave amplitude along the channel, the solution of which is determined by the driving condition at the wavemaker and the nature of the far field, from which the constants N and M are to be evaluated. Some of the possibilities are as follows.

(i) First we consider solutions whose character is similar to that of the linear mode below the cut-off frequency, cf. (3.2). These solutions decay at large distances from the wavemaker and so the constant M can be identified as being zero from conditions at infinity. (This implies that the phase is constant along the channel.) Furthermore the assumed nature of the solution at infinity implies, from (3.7), that $N = 0$.

The boundary condition (2.14) at the wavemaker can be written, for these solutions, as

$$R'(0) = -1, \quad \psi(0) = \pi,$$

and so the amplitude $R(0)$ at the wavemaker is given by

$$\left.\begin{aligned} \tfrac{1}{2}rR(0)^4 + pR(0)^2 + 1 &= 0, \\ \text{or} \qquad R(0)^2 &= (1/r)\{-p \pm \sqrt{(p^2 - 2r)}\}. \end{aligned}\right\} \tag{3.8}$$

There are two cases to consider.

(a) $r > 0$: this corresponds, in a given channel, to choosing the depth sufficiently large† and was the situation that applied for most of the experiments. When $r > 0$, real solutions to (3.8) are possible if $p^2 \geqslant 2r$ and $p < 0$, i.e. $p \leqslant -\sqrt{(2r)}$. For such frequencies, which we see are somewhat below the linear cut-off frequency, there are two possible values of $R(0)$ given by

$$R(0)_\pm = \{(1/r)[-p \pm \sqrt{(p^2 - 2r)}]\}^{\frac{1}{2}}. \tag{3.9}$$

Corresponding to each choice of $R(0)$ there is a solution for R, which decays monotonically with X, given implicitly by‡

$$X = \int_R^{R(0)} (-pS^2 + \tfrac{1}{2}rS^4)^{-\frac{1}{2}}\,dS. \tag{3.10}$$

† r changes sign when $\beta \approx 0.34$, and is positive when β exceeds this value.

‡ The actual solution for R is

$$R = \{(-2p/r)\,[1 - \{(1-u)/(1+u)\}^2]\}^{\frac{1}{2}},$$

where $$u = \{(1-U)/(1+U)\}\exp\{4(-p/r)^{\frac{1}{2}}X\} \quad \text{and} \quad U = (1 + rR(0)^2/2p)^{\frac{1}{2}}.$$

(*b*) $r < 0$, as is the situation when the water is sufficiently shallow. In this case there is a single real value of $R(0)$ possible, at all frequencies, given by

$$R(0) = \{(1/r)[-p-\sqrt{(p^2-2r)}]\}^{\frac{1}{2}}. \tag{3.11}$$

Again, the formula (3.10) describes the monotonely decaying solution $R(X)$ corresponding to this value of $R(0)$.

(ii) There is a class of solutions to the inviscid nonlinear equation which evidently corresponds to the linear propagating waves at frequencies above the cut-off value (cf. 3.2). These solutions are of the form

$$A_0 = R(0)\,\mathrm{e}^{-\mathrm{i}(CX+\chi)},$$

where $R(0)$, C, χ are real constants chosen to satisfy the differential equation and the boundary conditions. Accordingly, it follows from (3.5) that

$$-C^2+p+rR(0)^2 = 0,$$

and the boundary condition at the wavemaker (2.14) implies that

$$-\mathrm{i}CR(0)\,\mathrm{e}^{-\mathrm{i}\chi} = 1.$$

These two equations indicate that $\chi = -(\pi/2)\,\mathrm{sgn}\,C$ and that $R(0)$ is given by

$$rR(0)^4+pR(0)^2-1 = 0.$$

(*a*) $r > 0$. There is only one admissible value of $R(0)$, for any given p, which is

$$R(0) = \{[-p+\sqrt{(p^2+4r)}]/2r\}^{\frac{1}{2}}. \tag{3.12}$$

(*b*) $r < 0$. Real values for $R(0)$ are possible only if $p \geqslant 2\sqrt{(-r)}$, in which case there are two possible values given by

$$R(0)_{\pm} = \{[-p\pm\sqrt{(p^2+4r)}]/2r\}^{\frac{1}{2}}. \tag{3.13}$$

Typical sketches of the solution sets (3.9) and (3.12), for $r > 0$, are given in figure 2*a* and of the sets (3.11) and (3.13), for $r < 0$ are given in figure 2*b*.

These solutions pose some problems of interpretation, the nature of which we shall indicate for the case $r > 0$, when the water is relatively deep. When p is a sufficiently large negative number the solution set $R(0)_-$ given by (3.9) asymptotes to the solution given by the linear theory, and the distribution along the channel is similarly asymptotic to that resulting from the linear theory, so that we might expect this solution to apply, at least for sufficiently negative values of p. There is no decaying mode when $p > -\sqrt{(2r)}$, but for such frequencies (and indeed for all frequencies) there is the possibility of a 'propagating mode' given by (3.12). We should, however, interpret the term 'propagating mode' with some care because we have merely generalized the linear radiation condition by considering solutions of the form

$$R(0)\exp\{\mathrm{i}[t-(rR(0)^4+p)^{\frac{1}{2}}X-\tfrac{1}{2}\pi]\}$$

as outgoing waves: in linear theory this follows from the result that the phase and group velocities have the same direction. The solution set given by (3.12) asymptotes to that given by the linear model at frequencies well above cut-off, and thus it would appear to be reasonably well founded for sufficiently large values of p. On the other hand, for smaller values of p, and particularly when $p < 0$, there must be serious doubts about heuristic arguments of this kind. For example, when $p < 0$, a radiating mode of this kind is possible only because the amplitude is large enough for the

nonlinear frequency correction to predominate. It must accordingly be questionable as to whether or not such a solution could be joined on smoothly as a wave front, corresponding to that travelling with the group velocity from the linear theory (or its appropriate nonlinear generalization, whatever that may be), to a decaying solution. Indeed, to settle such a question, it would appear that one would have to consider an initial boundary-value problem for an equation of the form

$$A_{XX} - bA_{tt} + cA + dA^2A^* = 0,$$

which would require an extensive numerical investigation. Moreover, there is good reason to question the validity of such a model for the initial stages of the motions and *a fortiori* the predictions of such a model for the ultimate propagating wave solution that develops. For these reasons we did not consider that such a numerical investigation was warranted.

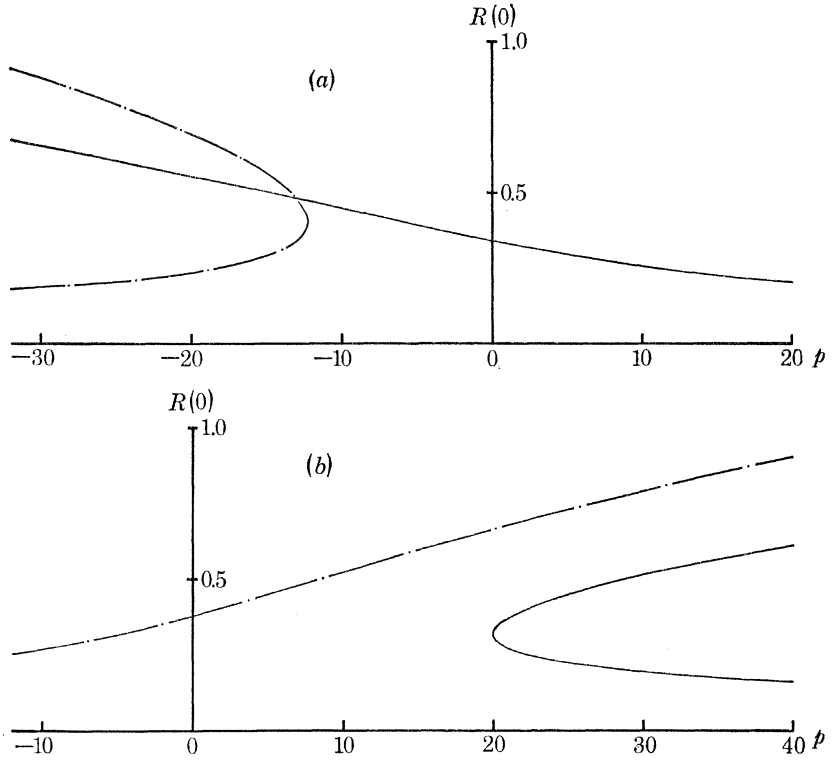

FIGURE 2. Some possibilities for the inviscid nonlinear response $R(0)$. (*a*) The case $r > 0$, $r = 74.96$: ——, radiating-wave solution (3.12); — · —, the monotone decaying solution (3.9). (*b*) The case $r < 0$, $r = -100$: ——, radiating-wave solution (3.13); — · —, the monotone decaying solution (3.11).

(iii) There is a two-parameter family of spatially periodic solutions to (3.7) depending on the nature of the far field. Solutions of this kind would appear to be relevant to the experimental observations, because wave absorption at beaches is never perfect and thus it is not feasible to specify *a priori* the values of M, N likely to be realized in any given experiment. This would mean, with regard to the laboratory experiments, that the values of N, M need to be determined empirically. One way of doing this is to measure the quantities $R(0)$, $\psi(0)$ and to relate M and N to these numbers through the boundary condition (2.14), which can be expressed as

$$[R'(0) + \mathrm{i}R(0)\,\psi'(0)]\,\mathrm{e}^{\mathrm{i}\psi(0)} = 1. \tag{3.14}$$

Using (3.6), we may write this as

$$R'(0)^2 + M^2 R(0)^{-2} = 1, \tag{3.15}$$

and

$$M^2 = R(0)^2 \tan^2 \psi(0)/(1 + \tan^2 \psi(0)). \tag{3.16}$$

Thus, knowing $R(0)$ and $\psi(0)$ we can determine M^2 from (3.16) and then find N from (3.15) and (3.7). Then, for a given $R(0)$, we can determine the function $R(X)$ by an integration of (3.7).

For the deep-water experiments, $r > 0$, we can, however, determine the supremum and infimum for R without having to carry out this integration. Since R is a real-valued, positive, function it follows from (3.7) that

$$R' = \pm R^{-1}\{-\tfrac{1}{2}rR^6 - pR^4 + NR^2 - M^2\}^{\frac{1}{2}}, \tag{3.17}$$

and so, for R' to be well defined for each X, this implies that R must lie in the interval $[R_L, R_U]$ on which the radical of (3.17) takes positive values. Thus R_L^2, R_U^2 are given by the two positive roots of the polynomial $\{-\tfrac{1}{2}rY^3 - pY^2 + NY - M^2\}$.

By using these ideas it is shown, in appendix A, that the inviscid model (3.4) cannot give an adequate description of the experimental observations.

3.3.2. *Dissipative model*

As indicated above, it eventually became apparent to us that the inclusion of the dissipative term would be essential if the theoretical model were to stand any chance of describing the major features observed experimentally. However there seemed to us little hope of achieving an analytic treatment of equation (2.22) and so we decided to look for a numerical solution by methods which would, at least, permit a qualitative analysis of the possible solution structures.

Fortunately it is possible to arrange the numerical calculations so that they can proceed as solutions to an initial-value, rather than to a boundary-value, problem. This happens because, with damping present, all the solutions of the differential equation tend to zero as $X \to \infty$. Thus, for sufficiently large X, the solutions necessarily are dominated by the linear equation (with dissipation) and must be of the form given in (3.3). We shall use this feature to provide a starting point for the numerical computations.

Using the substitution $A_0 = R\exp(i\psi)$ in the model equation (2.22) we have that

$$R'' - R\psi'^2 + pR + rR^3 = 0, \tag{3.18a}$$

and

$$(R^2\psi')' = -qR^2. \tag{3.18b}$$

For the numerical calculations it is convenient to transform these equations to new variables and in our computations we have used two different versions.

(i) Let R be the independent variable, and use new dependent variables, V and W, defined by

$$V = R', \quad W = \psi'. \tag{3.19}$$

In terms of these new variables equations (3.18) transform to

$$\frac{\mathrm{d}}{\mathrm{d}R}(\tfrac{1}{2}V^2) = (W^2 - p - rR^2)\,R, \tag{3.20a}$$

and

$$\frac{\mathrm{d}W}{\mathrm{d}R} = -q/V - 2W/R. \tag{3.20b}$$

Given initial values for V and W, for some R, these equations can be integrated numerically. The initial conditions are derived from the far field where it is assumed that the wave amplitude

R is small, and that the linear dissipative model accordingly gives a good approximation to the motions. Thus from (3.3) we have that

$$V = vR, \quad W = q/2v, \tag{3.21}$$

where $$v = [\tfrac{1}{2}(-p+\sqrt{(p^2+q^2)})]^{\frac{1}{2}},$$

and these were used as the initial values for the integration of (3.20). This integration procedure can be continued until the point is reached at which V vanishes. However, to retain numerical accuracy, it is necessary in practice to curtail the integration before this happens and change to new variables, for which this singularity is obviated.

(ii) To continue the integration through points at which $\mathrm{d}R/\mathrm{d}X$ vanishes we use as the independent variable the quantity $S = R^2W$ (which we see from (3.18b) to be a strictly monotonic function of X), and we let the dependent variables be V, R. In terms of these variables, equations (3.18) become

$$\mathrm{d}V/\mathrm{d}S = \frac{rR^6+pR^4-S^2}{qR^5}, \tag{3.22a}$$

and

$$\mathrm{d}R/\mathrm{d}S = -V/qR^2. \tag{3.22b}$$

Therefore, having used (3.20) to initiate the numerical integration and achieve moderate values of R, we can then transfer to equations (3.22) for which the integration can be continued as long as desired.

Accordingly we have converted the computation to one of solving an initial-value problem, starting from the known solution in the far field given by the linear dissipative theory. The origin for the computed solution is determined by a point at which the boundary condition (2.14) (or equivalently 3.14) is satisfied, and the distance from the origin can then be determined by an additional quadrature. Thus, for a given far field, there may be more than one point of the solution set at which the boundary condition (2.14) is satisfied, and each such point represents a possible origin for a solution to the forced motion. The boundary condition (2.14) can be separated as

$$J \equiv V^2+R^2W^2-1 = 0 \quad \text{(case (i))}, \quad \text{or} \quad J \equiv V^2+S^2R^{-2}-1 = 0 \quad \text{(case (ii))},$$

with the original equation (3.14) determining $\psi(0)$ when the other terms are known.

3.3.3. *Numerical solutions*

In carrying out the numerical computations it is convenient to introduce a scaling

$$A_0(X) = q^{-\frac{1}{2}}\mathscr{A}(q^{\frac{1}{2}}X),$$

so that (2.22) transforms to

$$\mathscr{A}''+(p+\mathrm{i}+\tilde{r}\mathscr{A}\mathscr{A}^*)\mathscr{A} = 0, \tag{3.23}$$

where $\tilde{p} = p/q$ and $\tilde{r} = r/q^2$, and so the solutions need to be obtained only for two families of parameters. These solutions to the scaled equation (3.23) are equivalent to those obtained by the methods described above, by setting $q = 1$.

To start the computations, a value of $|\mathscr{A}|$ was chosen, usually 10^{-4}, and the initial conditions for V and W were determined from (3.21). Equations (3.20) were then integrated by means of a Runge–Kutta procedure and the sign of J, which initially is negative, was monitored. The zeros of J determine the possible values of the amplitude at the wavemaker. (Incidentally, the first of (3.19), or an equivalent form when using the independent variable S, was carried in the integration so that the distribution along the channel could be reconstructed once the value $R(0)$ had

been found.) The integration was allowed to proceed until V started to become small, at which point the integration was continued by means of (3.22).

As mentioned above, J initially is negative, and for large values of R (or S in case (ii)) it was found to be a large positive number. Therefore, the number of possible values of $R(0)$, counted with their multiplicity, is odd. In practice we carried on the numerical integration far enough to rule out the possibility of other solutions. An interesting feature of these solutions is that, if there is more than one value of $R(0)$ corresponding to a given set of parameters, the solutions have exactly the same shape at large distances from the wavemaker. The additional solutions, apart from a translation, agree with the first solution at large distances, and differ from it only in the vicinity of the wavemaker.

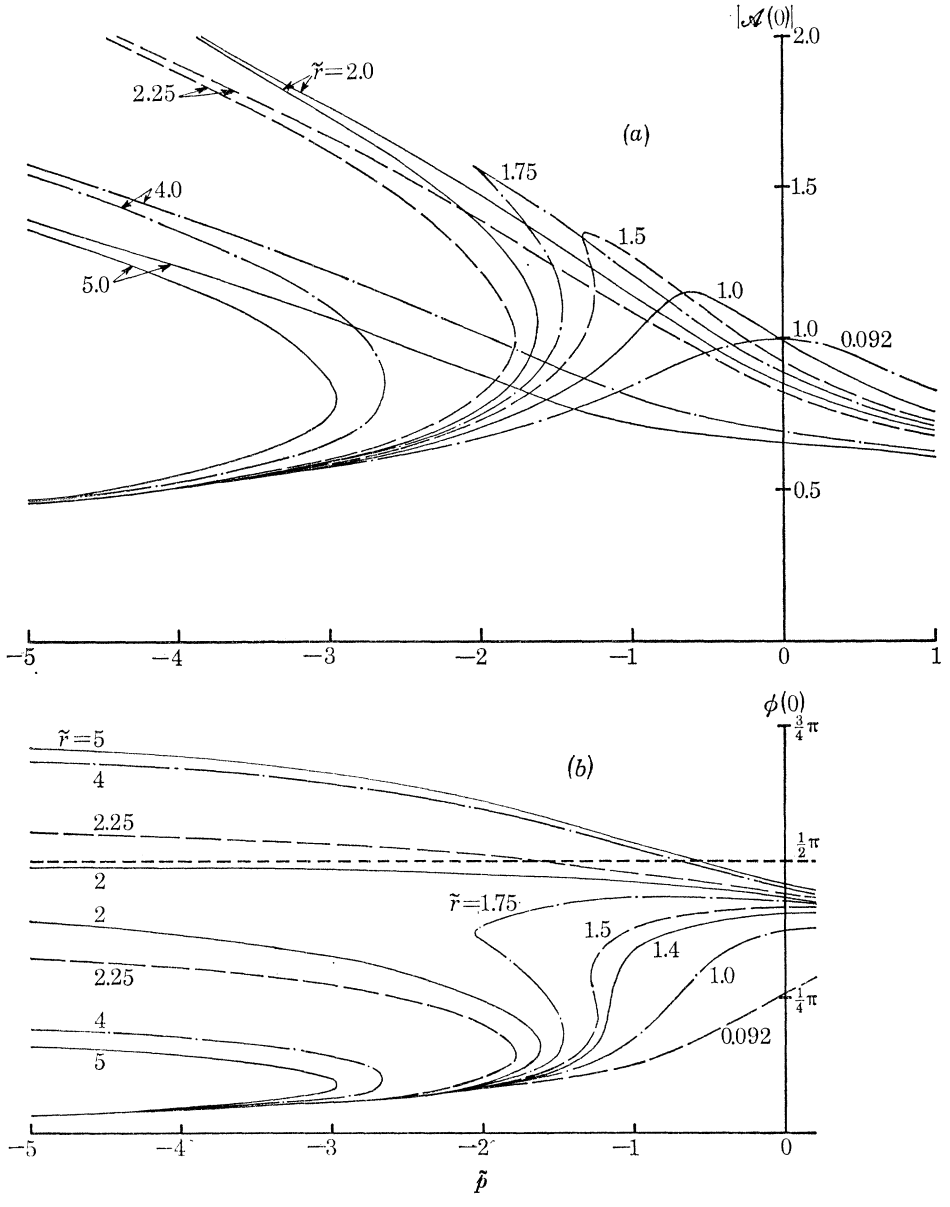

FIGURE 3. The response for the nonlinear viscous model according to the numerical computations, for various values of $\tilde{r} > 0$. (*a*) The amplitude response $|\mathscr{A}(0)|$. (*b*) The phase $\phi(0)$ $(\equiv \pi - \psi(0))$.

The results of the numerical computations are summarized in the graphs given in figures 3 (the case $r > 0$) and figure 4 (the case $r < 0$). In figure 3*a* the amplitude at the wavemaker is shown as a function of $\tilde{p}$ for various values of $\tilde{r}$, and in figure 3*b* we give the phase of the waves at the wavemaker. It was of interest to us that these results showed very little resemblance to those of the inviscid theories described above or to the theory of Ockendon & Ockendon (1973). The reason for this appears to be linked to the dissipative term which, no matter how small it is relative to the other terms, plays a crucial rôle in the structure of the solutions when $(\tilde{p} + r\mathscr{A}\mathscr{A}^*)$ is small.

The curves in figure 3*a* for small values of $\tilde{r}$ correspond to the situation in which the dissipative effects dominate over the nonlinear effects and the solutions for the wave amplitudes are similar

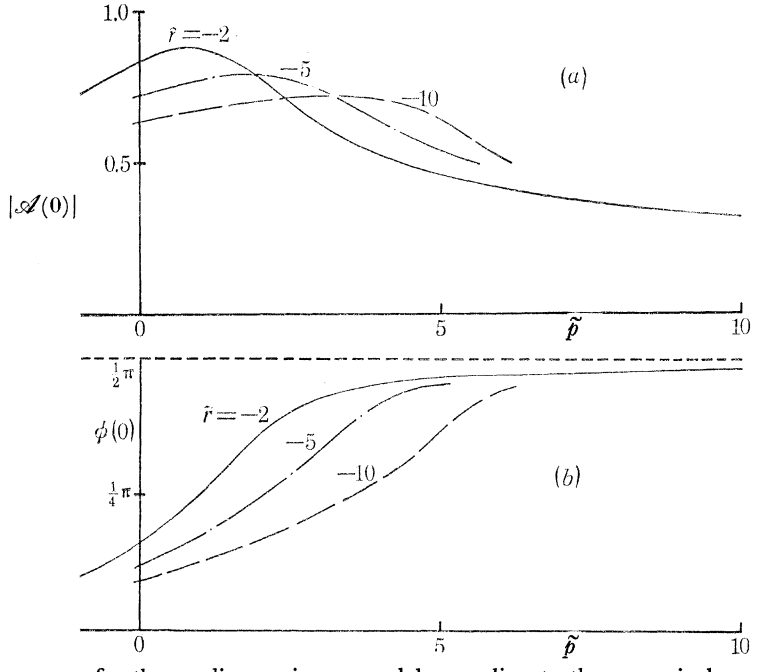

FIGURE 4. The response for the nonlinear viscous model according to the numerical computations, for various values of $\tilde{r} < 0$. (*a*) The amplitude response $|\mathscr{A}(0)|$. (*b*) The phase $\phi(0)$.

to those shown in figure 1. As $\tilde{r}$ increases the maximum response occurs at more negative values of $\tilde{p}$ until, at a value of $\tilde{r}$ of about 1.43, the computations indicated that three solutions were possible. For values of $\tilde{r}$ between 1.43 and 2.000 these three possible solutions were obtained only over a finite interval in $\tilde{p}$. But for $\tilde{r} \geqslant 2.000$ the computations suggest that there are three solutions no matter how large a negative value of $\tilde{p}$ is chosen.† The case in which $\tilde{r} = 2.0$ appears to be the largest value of r for which the phase $\phi(0)$ $(\equiv \pi - \psi(0))$ of the waves at the paddle is less than $\frac{1}{2}\pi$ for all values of $\tilde{p}$, as indicated in figure 3*b*. The computations for $\tilde{r} < 0$, as shown in figure 4, yielded only one solution for all values of $\tilde{p}$. In this case the phase $\phi(0)$ lay in the interval $[0, \frac{1}{2}\pi]$.

Although the results of these computations were quite unexpected to us, especially the differences between the solution sets for $\tilde{r} > 0$, it is just these kinds of differences that are needed to

† A computation made at $\tilde{r} = 1.95$ showed that the three solutions were no longer present when $\tilde{p} = -8.0$; for $\tilde{r} = 1.99$ they were present at $\tilde{p} = -8.0$ but not when $\tilde{p} = -15.0$; when $\tilde{r} = 1.999$ the three solutions persisted beyond $\tilde{p} = -20.0$ but not as far as $\tilde{p} = -40.0$. For $\tilde{r} = 2.000$, the computations indicated three solutions were still possible at $\tilde{p} = -40.0$.

explain the experimental observations. Only two solutions, at the most, were observed in the experiments and presumably, in those cases where more than one state was possible, the third state predicted by the numerical computations is not stable, and therefore not seen experimentally. For these reasons, we have indicated in the work described below only those portions of the solution set that appear to be relevant to the observations, however we should stress that we do not have any proof that the omitted portions do in fact correspond to unstable states.

Details of the computed wave amplitudes along the channel, which again are radically different from those predicted by the inviscid theory, are given below in conjunction with the empirical data.

4. Experimental apparatus

The experiments to be described were made in a rectangular channel of width 29.55 cm and length 6 m, which usually contained about 17 cm of water. For these experiments the linear cut-off frequency γ, as defined in (2.6), was 1.7260, which corresponded to a period of about 0.63 s. The ' bandwidth ' of the response was roughly 0.0075 s, so that, in order to investigate the structure of the response curve, it seemed necessary to have a wavemaker whose frequency was stable to within about 0.0001 s for the duration of the experiment, and to have a channel whose width and depth were uniform to close enough tolerances that ' local ' values of γ varied by no more than 1 part in 6000, in line with the stability of the wavemaker drive. According to (2.6) these latter requirements imply that the width of the present channel should be uniform to within 0.01 cm, and the depth should vary by no more than 0.03 cm. Thus, a channel was built specially for this experiment, with glass walls and a glass bottom in which the width was uniform to within 0.005 cm and the depth varied by no more than 0.030 cm. (A discussion of why these tolerances were so important is given in appendix A.)

At one end of the channel a sloping beach was used to absorb progressive waves, and at the other end a plane flap, spanning the channel, was used to excite the wave motions. This flap was mounted on a vertical shaft passing through the centre of the channel, and could be rotated about the axis determined by this shaft. The gaps between the flap and the walls, and the flap and the floor of the channel were filled with foam plastic, attached to the flap, in order to reduce leakage past the wavemaker to negligible proportions. This flap was driven in rotational oscillations of about $\frac{1}{2}°$ in amplitude by an electromagnetic vibrator which was driven in the following way. A square wave was taken from a low-powered oscillator with suitable stability characteristics (namely that the period of the waveform should vary by less than 1 part in 6000 over an interval of about 2 h). This waveform was used to switch a d.c. power supply connected to the vibrator so that the vibrator received a periodic forcing whose stability properties were determined by the low-powered source. But the harmonic content of the waveform from the vibrator was very large, and this was removed by driving the vibrator through a mechanical filter. The filter was simply a mass at the end of a cantilevered beam, the position of the mass being adjustable so the resonant frequency of the filter could be tuned to the operating frequency determined by the oscillator. The harmonic content of the motion at the paddle was so small, compared with the fundamental mode, that it was not discernable in the waveform at the paddle.

Thus, the driving method proved to be very reliable and easy to use. Its operating frequency and stability characteristics were determined completely by the low-powered, stable, oscillator so that fine adjustments to the frequency could easily be made, and long-term drifting of the operating frequency were essentially eliminated. In addition, the use of the mechanical filter meant

that an extremely good waveform could be obtained from a reasonably small vibrator, thereby avoiding the use of heavy and cumbersome driving equipment that might otherwise have been necessary at these frequencies.

The amplitude of the wavemaker oscillations was determined from the displacement of a dial gauge bearing directly on the wavemaker. The frequencies employed were low enough that the gauge faithfully followed the motion of the wavemaker and the two extremities of the movement of the gauge's needle could easily be read. Thus the amplitude of the wavemaker could be followed throughout the experiment: it was measured to an accuracy of about 0.2 % and remained steady throughout any experiment to within 1 %.

The operating frequency was measured with an electronic counter, triggered by the input waveform to the vibrator. Throughout each experiment a careful watch was kept on the operating frequency to ensure that it did not vary by more than 1 part in 6000 .

The amplitudes of the waves were estimated from measurements of the wave crests. These measurements were made by carefully lowering a finely machined pointer until it just broke the surface of the water, from which the height of the pointer above the still-water level was determined. The pointer was mounted on a carriage and could be moved to any desired position in the channel. This method gave the height of the wave crests above the still-water level to within 0.04 mm. In addition, some measurements of the wave troughs were made in a similar way by using a hook gauge.

The experimental procedure was as follows: the desired operating frequency was located on the oscillator; the power to the vibrator was connected and its magnitude was gradually increased until the desired amplitude of the wavemaker movement was reached. Usually the steady state, as indicated by the wave amplitude, would be achieved within a period of a few minutes and persisted for the duration of the experiment.

Some rough estimates were made of the damping of free waves with $k = 0$. These measurements were made in connection with some of the early work in this study (cf. appendix A) and were carried out in a tank of similar cross section to that described above, but of much smaller length. To make these measurements of the decay rate of free waves a false, plane, end was placed in the tank about 1.5 m from the wavemaker and two-dimensional standing waves (with their crests along the channel) were generated by gently rocking the tank from side to side, and then stiffening the structure laterally so that no further movement was possible. The amplitude of these waves was then measured as a function of time (details of similar measurements are given in Barnard & Pritchard 1972) and their frequency was determined. From these measurements the values of the constants C_3 and C_4 of equation (2.21) could be estimated, as indicated in § 3.2, but these should only be used as a guide to the actual values of C_3 and C_4. The reason for this is that the tank in which the damping measurements were made was not constructed to the same accuracy as that used for the main experiments, so that the estimate of C_4 is likely to be considerably in error. Also the false end was placed not very far from the wavemaker and therefore the constant C_3 was almost certainly overestimated.

5. Experimental results

The experimental results for the wave amplitudes are described in terms of the (dimensionless) quantities actually measured, rather than presenting them in terms of the scaled variables. However, it has been convenient to leave the independent variable X in its scaled form, i.e.

$X = \epsilon^{\frac{1}{2}}x$, where x is the distance from the wavemaker. Then, in terms of the above theory, the surface displacement at the crest of the wave is related to $R(X) = |A_0(X)|$ by

$$\zeta(X) = \epsilon^{\frac{1}{2}}\gamma \cos \pi y\, R(X), \tag{5.1}$$

where y is the distance from the wall of the channel (cf. § 2).

The frequency ω is related to the parameter p defined by (2.22) and the quantities σ, δ introduced in § 3.2 by

$$p = (\omega^2 - \sigma^2 + \delta^2)/\epsilon a.$$

Phase measurements are described relative to the rearmost position of the paddle during its cycle, and we shall define this quantity to be $\phi(X)$, where $\phi(X) \equiv \pi - \psi(X)$ in terms of the theory described above.

All the measurements, unless stated otherwise, were made at a distance of 5.0 cm from one of the walls of the tank, so that $\pi y = 0.532$. Similarly the ratio $\beta(= d/b) = 0.5777$, except for the results of § 5.4 and the appendixes (in which case it was only slightly different from 0.5777). The corresponding value of r, as defined by (2.22), is 74.96.

5.1. *The response at a given X*

Shown in figure 5 are the results of measurements, made at $X = 0.069$, of the amplitude of the wave crests for a number of different amplitudes of the wavemaker. (Since the data are given in dimensionless form it is worth noting that the largest wavemaker amplitude was about 0.6°, and for this forcing the largest waves observed had an amplitude of about 28 mm.) When the amplitude of the wavemaker was increased the largest observed response increased, and was found to occur at smaller and smaller values of ω. For the two largest values of ϵ used in these experiments it was possible, at some frequencies, to obtain two different kinds of response. For example, when $\epsilon = 0.01045$ and $\omega = 1.7162$, it was found that, on increasing the amplitude of the wavemaker up to the desired value, the wave amplitude at $X = 0.069$ assumed the smaller of the two values indicated in the graph (see point A). If however the amplitude of the wavemaker was increased the waves built up to a much larger size and on reducing the amplitude of the paddle to $\epsilon = 0.01045$ it was found that the state (B) characterized by the much larger amplitudes persisted. (There is a curious kink, or dip, in the data for $\epsilon = 0.01045$ at frequencies near the cut off. This feature will be discussed below in § 5.3.)

The wave response when $\epsilon = 0.01045$ is compared, in figure 6, with some of the theories described in § 3. The linear theories do not appear to give a very good description of the results, but the nonlinear solutions (3.9) (taking the R_- branch) and (3.12) appear to give a reasonably good description of the data. However, more complete comparisons with the observations (to be given below) indicate that these theories cannot give a satisfactory description of more critical aspects of the experimental situation.

Shown in figure 7 is a comparison of the response at $X = 0.069$ with predictions from the dissipative model obtained by the numerical integration described in § 3.3. Unfortunately there is a certain amount of arbitrariness in this comparison because we are not able to specify *a priori* the magnitude of the dissipative effects. These effects manifest themselves in two ways: one way is through the constant C_3 (see (2.21)) which effectively modifies the cut-off frequency; the other influence is through the constant C_4 (or its equivalent, the parameter q of (2.21)) the magnitude of which, according to the numerical experiments, has a very important effect on the motions realized in the laboratory experiments. For the purposes of the present investigation we have

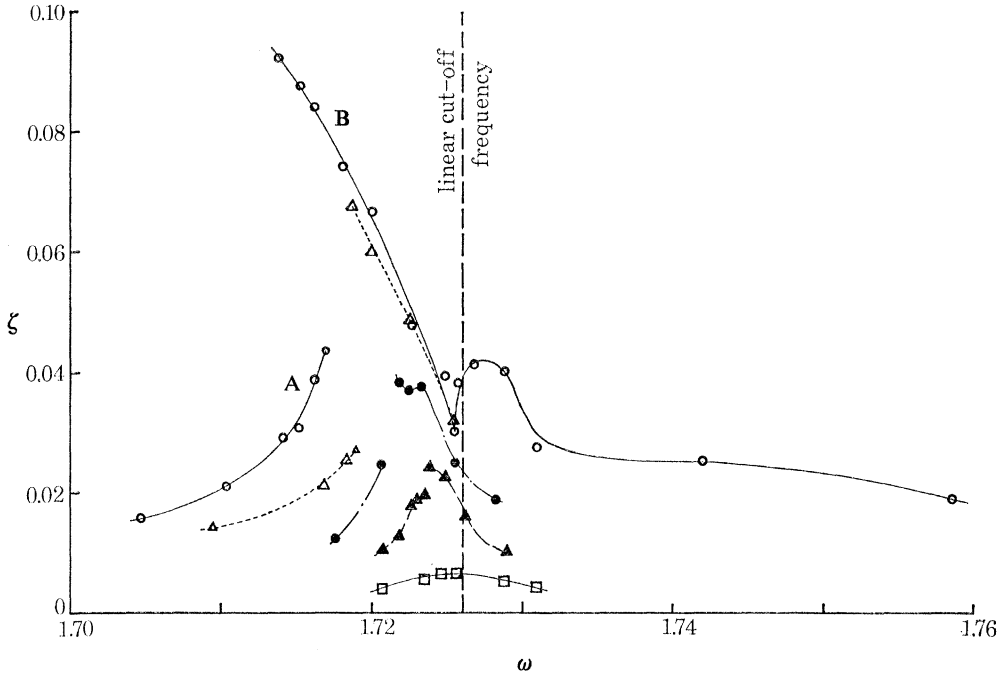

FIGURE 5. The height, ζ, of the wave crest above the still-water level as related to the wavemaker frequency ω, for various values of the wavemaker amplitude. ○, $\epsilon = 0.01045$; △, $\epsilon = 0.00783$; ●, $\epsilon = 0.00527$; ▲, $\epsilon = 0.00316$; □, $\epsilon = 0.00158$. These measurements were made at $X = 0.069$.

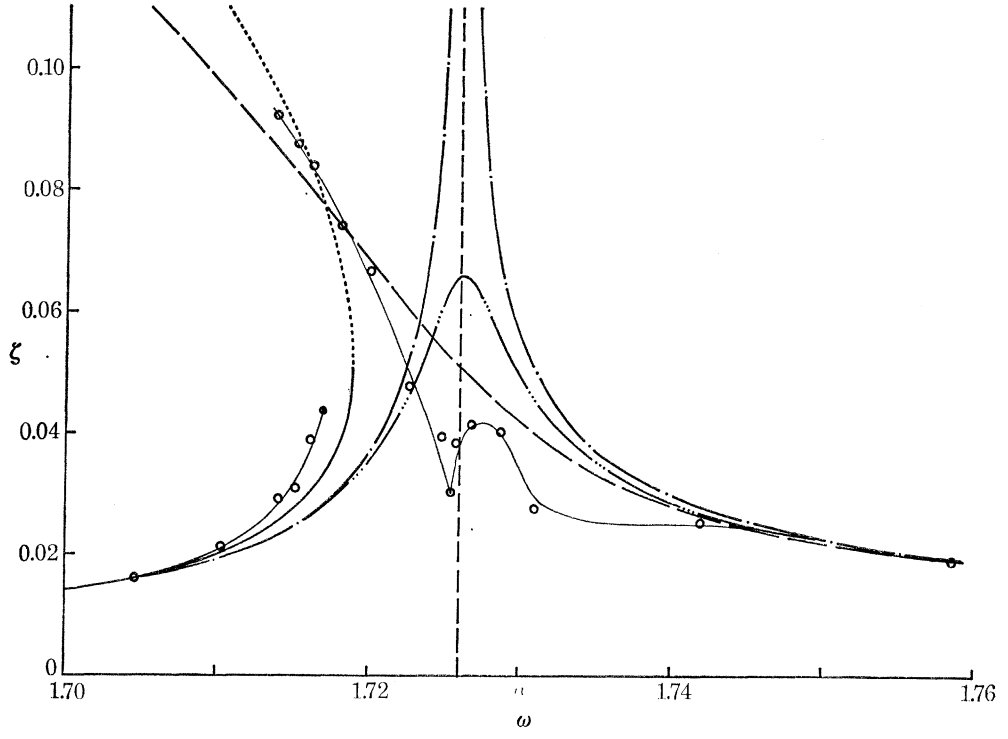

FIGURE 6. A comparison of the experimental results of figure 5, for $\epsilon = 0.01045$, with various theories. —·—, linear inviscid theory (3.2); —···—, linear viscous theory, $\epsilon q = 0.045$, (3.3); ——, nonlinear inviscid theory (3.9, the R_- branch of the monotone decaying solution); - - - - - -, nonlinear inviscid theory (3.9, the R_+ branch of the monotone decaying solution); — — —, nonlinear inviscid theory (3.12, radiating-wave solution).

chosen a particular value for q and used that for all subsequent comparisons. (The way in which q was chosen is outlined in appendix B.) Thus, for the comparison in figure 7 we have assumed that $\epsilon q = 0.046$; also the theoretical value of the cut-off frequency has been reduced by 0.0014.† Note that, in drawing the theoretical curves for figure 7, we have omitted a subset of each of the solution sets in the belief (derived from the comparison with the experimental results) that it corresponds to an unstable mode.

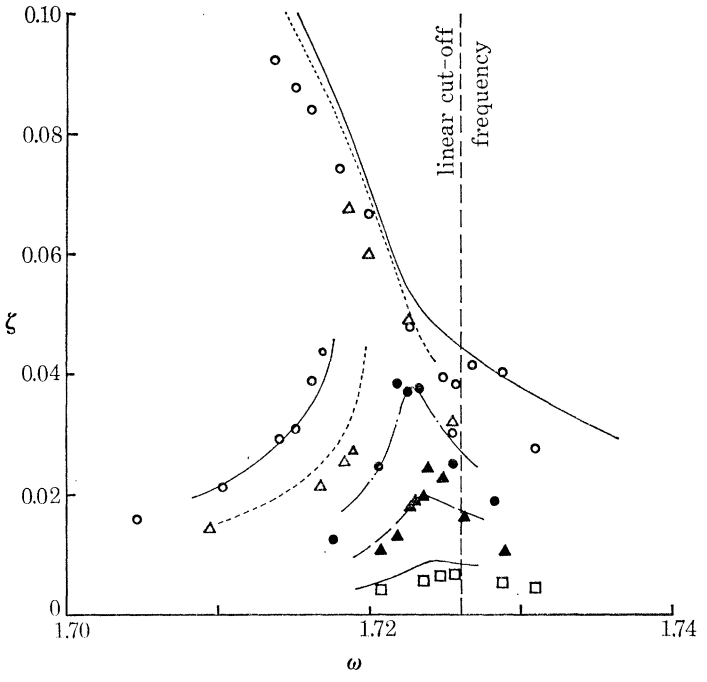

FIGURE 7. A comparison of the experimental results with the numerical solutions of the nonlinear dissipative model (2.22), for $\epsilon q = 0.046$. ○, ——: $\epsilon = 0.01045$; △, - - - - - -: $\epsilon = 0.00783$; ●, —·—: $\epsilon = 0.00527$; ▲, — —: $\epsilon = 0.00316$; □, ——: $\epsilon = 0.00158$. Note that there has been a relative translation of the frequency scales of 0.0014.

5.2. *The phase at* $X = 0$

Some measurements were made of the phase, $\phi(0)$ of the waves at the wavemaker and the results of these for the three largest values of ϵ are shown in figures 8*a*, *b*, *c*. Also shown in this figure are the theoretical values of $\phi(0)$ obtained from the numerical computations. One important feature to emerge from these measurements were the values for $\phi(0)$ in excess of $\frac{1}{2}\pi$ at some of the frequencies when $\epsilon = 0.01045$ and $\epsilon = 0.00783$. This was not observed at any other values of ϵ (an example of which is given in figure 8*c*) and is predicted only by the nonlinear dissipative model.

The quantitative agreement between the experimental results and the numerical computations is not very close, but the qualitative features of the observations are described very well by the theory. Also, phase factors can be very sensitive to small influences (an example of which is described in appendix A), and thus the comparisons shown in figure 8 are likely to be a very sensitive test.

† This is the only occasion on which a frequency adjustment has been made.

5.3. *The structure along the channel*

In figure 9 we give some examples of the variation of the wave amplitude along the channel for the wavemaker amplitude $\epsilon = 0.01045$. Also shown in this figure are the results of numerical computations made at roughly the same values of p as those at which the experiments were carried out. These have been included to show how the nonlinear dissipative model predicts a

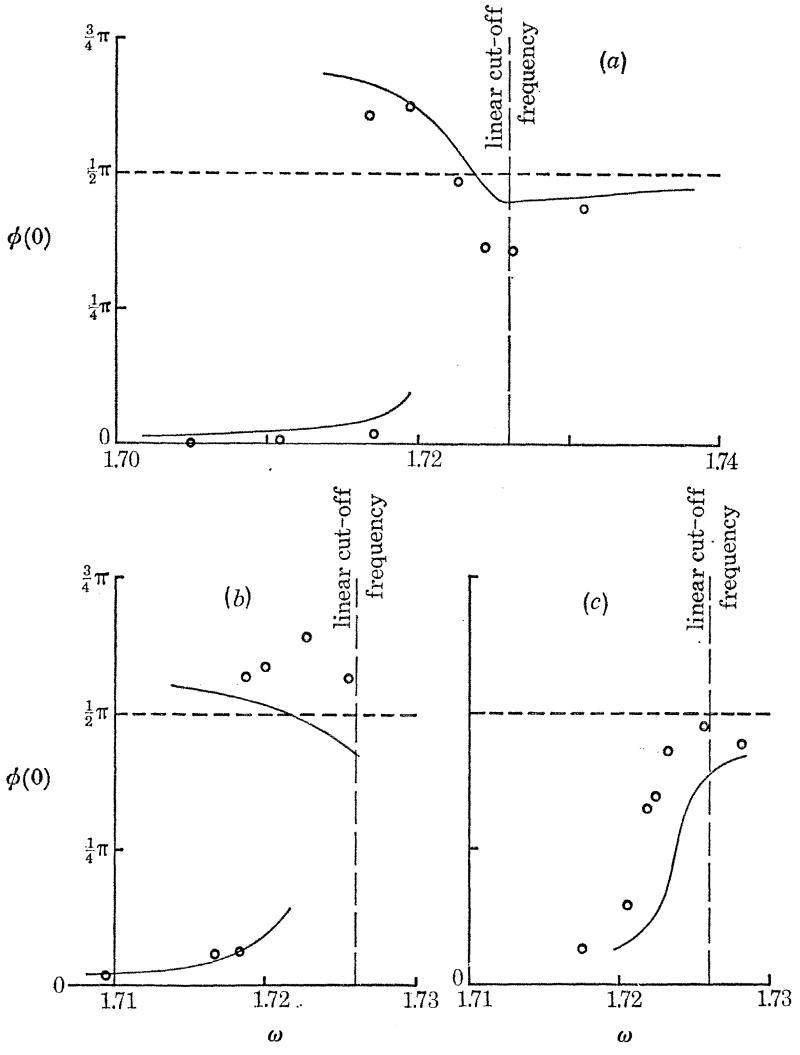

FIGURE 8. The phase $\phi(0)$ of the waves at the wavemaker, as related to the frequency ω, is compared with the predictions from the nonlinear dissipative model (2.22), for $\epsilon q = 0.046$. (*a*) $\epsilon = 0.01045$; (*b*) $\epsilon = 0.00783$; (*c*) $\epsilon = 0.00527$.

distribution along the channel with similar characteristics to those observed experimentally, whereas the models without dissipation give a very poor description of this data (see below in figure 11 and also in appendix A).

For figure 9*a* the frequency was well below the cut-off frequency and only one state was observed. But when $p = -19.02$ two stable motions were observed experimentally. One of these had a much larger amplitude than the other in the vicinity of the wavemaker, but the amplitude

of both motions decayed rapidly towards zero as X increased. The numerical solutions display similar properties.

As the frequency increases we have again the situation in which only one stable motion was observed at a given value of p, as shown in figure 9*d*. Also it is evident in figure 9*d*, and at larger values of p as well, that the wave amplitude initially increased with X, passed through a maximum value and then decreased towards zero. This feature is also displayed by the numerical

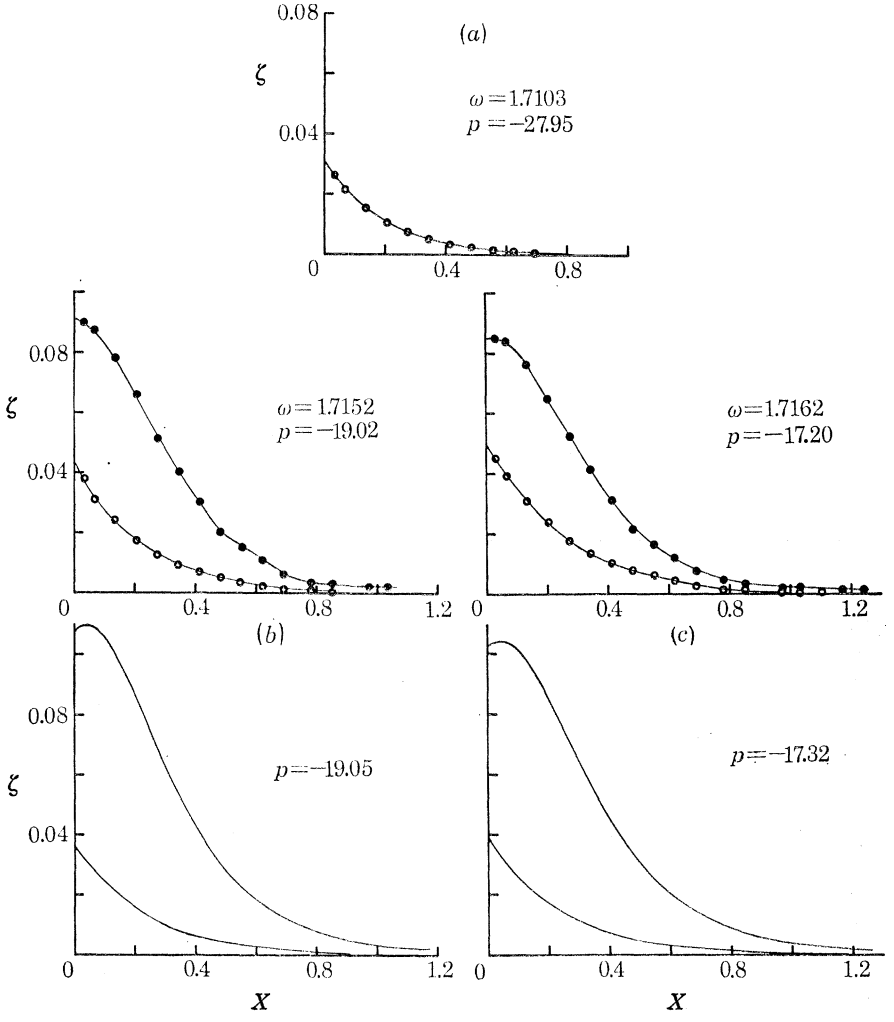

FIGURE 9. The amplitude response ζ along the channel for $\epsilon = 0.01045$ and for various values of ω. The upper set of graphs are the experimental results and the lower set are the predictions from the nonlinear dissipative model with $\epsilon q = 0.046$. There are no theoretical graphs given in figures 9 *a*, *h*.

solutions. However, as p was increased to values near zero the decay of the wave amplitude with X became much less rapid and the motions spread, at significant levels, all the way to the beach (the toe of which began at $X = 1.55$ for figure 9). Thus the response curves shown in figures 9 (*f*), (*g*), (*h*), and (*i*) almost certainly have a significant standing-wave component. This feature is particularly noticeable in figures 9*h*, *i*.†

† In §5.1 reference was made to a sharp 'dip' in the amplitude response at $X = 0.069$ (for the wavemaker amplitude $\epsilon = 0.01045$) very near the cut-off frequency. It is possible that this feature is connected with the standing-wave component which can either add to or subtract from the primary forced motion near $X = 0$, depending on the relative phases there. This property is illustrated by the results in figures 9*f*–*i*.

Some measurements of the variation of the phase along the channel, for the same wavemaker amplitude as that pertaining to figure 9, are given in figure 10. For $p \approx -27$ (cf. figure 9*a* for the amplitude response) we see in figure 10*a* that ϕ was small, and the phase of the waves did not vary much along the channel. When $p \approx -16$ (cf. figure 9*c* for the amplitude response) one of the two observed states had $\phi(0)$ small and the other had $\phi(0)$ slightly in excess of $\frac{1}{2}\pi$, and in each case

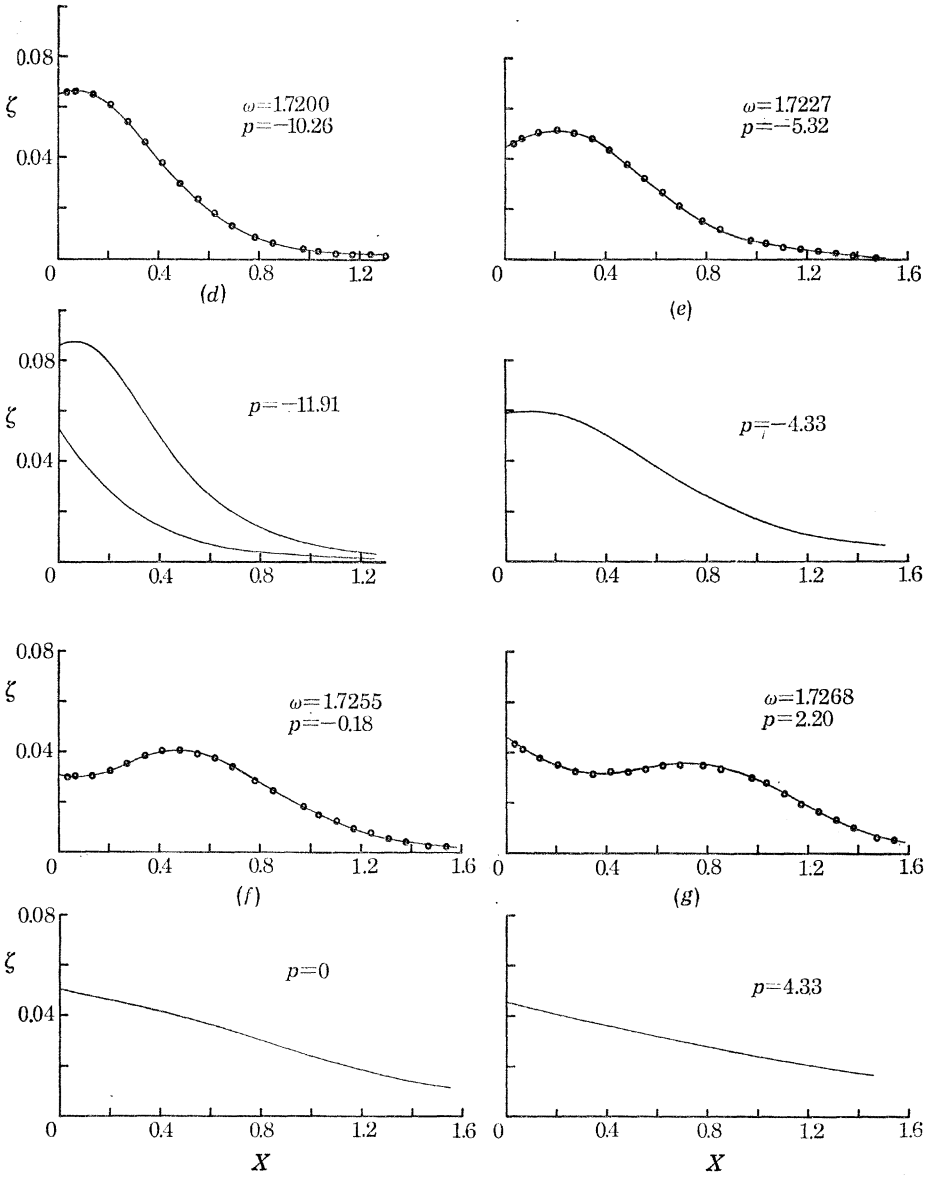

FIGURE 9 *d–g*. For legend see preceding page.

there was only a small variation of ϕ along the channel, as indicated in figure 10*b*. At larger values of p (e.g. for $p \sim -5$, as shown in figure 10*c*) the variation in ϕ along the channel was much larger than at the more negative values of p.

The amplitude response for $\epsilon = 0.00783$, similar to that shown in figure 9 for $\epsilon = 0.01045$, is given in figure 11. The structure of these motions displayed similar properties to those for the

larger value of ϵ. In figure 11*a* we have included the range of values $[\zeta_L, \zeta_U]$† for the solution to the inviscid model equation which satisfies the observed values of $\zeta(0)$ and $\phi(0)$ at this frequency, as described in §3.3.3. It is clear from these results that the inviscid model cannot be used to describe the experimental results.

The experimental results for the amplitude response along the channel, together with the theoretical predictions, for $\epsilon = 0.00527$, $\epsilon = 0.00316$ and $\epsilon = 0.00158$ are shown respectively in figures 12, 13 and 14.

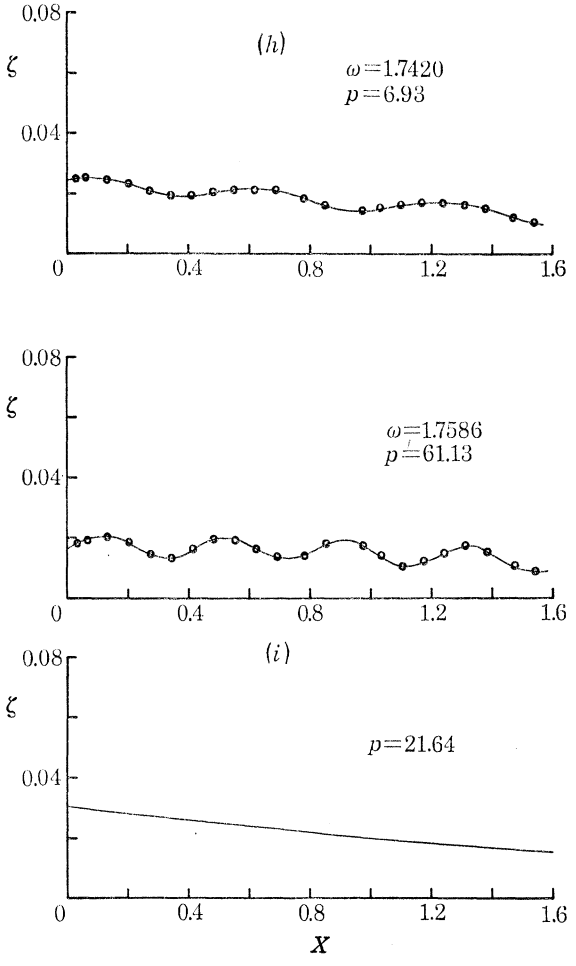

FIGURE 9 *h–i*. For legend see p. 113.

5.4. *The response as a function of depth*

In the course of making the experiments described in appendix A some measurements were made of the response near the cut-off frequency for different depths of liquid. The depths were chosen so that the quantity r defined by (2.22) was greater than zero, approximately equal to zero and less than zero. The results of these measurements are given in figure 15 and it is evident that the response is quite different for each of the different values of β. At the depth at which the parameter r changes sign, i.e. at $\beta = 0.340$, the arguments used in §2 cannot be expected to give correct estimates of the order of the solution and accordingly the analysis is not necessarily expected to be applicable in this case.

† The quantities ζ_L, ζ_U are related to R_L, R_U of §3.3 via (5.1).

For the case in which $r < 0$ the response was much smaller than in the other cases and is in general agreement with that found from the numerical computations (see figure 4).

5.5. *The structure across the channel*

Also in the course of making the experiments described in appendix A we measured the amplitude of the crest and the trough of a wave in a plane across the channel and the results of one such set of data are given in figure 16. The fact that the magnitude of the depression of the wave differs substantially from that of the elevation confirms once more that the nonlinear effects were important in determining the structure of the motions.

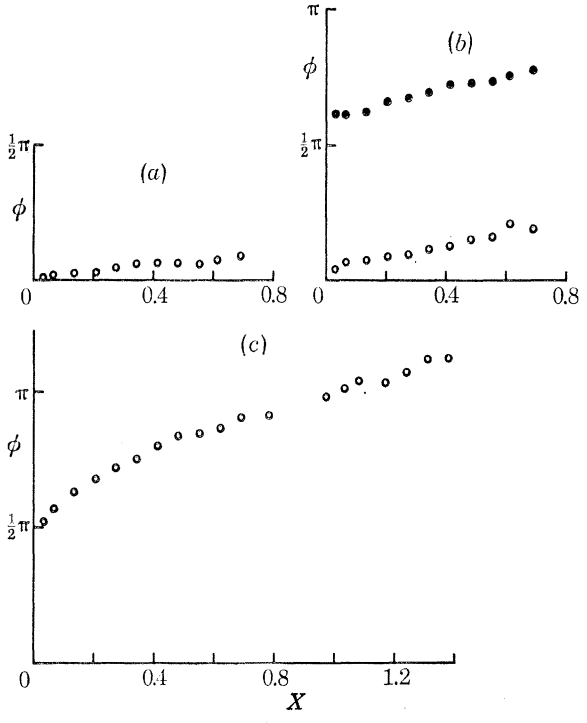

FIGURE 10. Experimental results for the phase ϕ of the waves as a function of distance along the channel, for $\epsilon = 0.01045$. (*a*) $\omega = 1.7109$, $p = -26.86$; (*b*) $\omega = 1.7170$, $p = -15.74$; (*c*) $\omega = 1.7227$, $p = -5.32$.

5.6. *Conclusion*

We think the results of this investigation demonstrate fairly convincingly that the nonlinear inviscid model cannot give a satisfactory overall description of the empirical observations. In particular, the structure of the wave motions along the channel cannot be predicted reliably by this model, and also the phase predictions are in poor agreement with the observations.

However, the inclusion of dissipative effects in the theoretical model has a profound influence on the structure of the wave motions, as indicated by the numerical computations described in § 3.3. These differences give a significant improvement in the overall agreement between the predictions from the theoretical model and the experimental results. Certainly there are still quantitative differences between the theory and the experiments, but we feel that, given the many approximations involved in deriving the model equation, the general agreement is good enough to suggest that the theoretical model is of considerable value in interpreting the experimental situation.

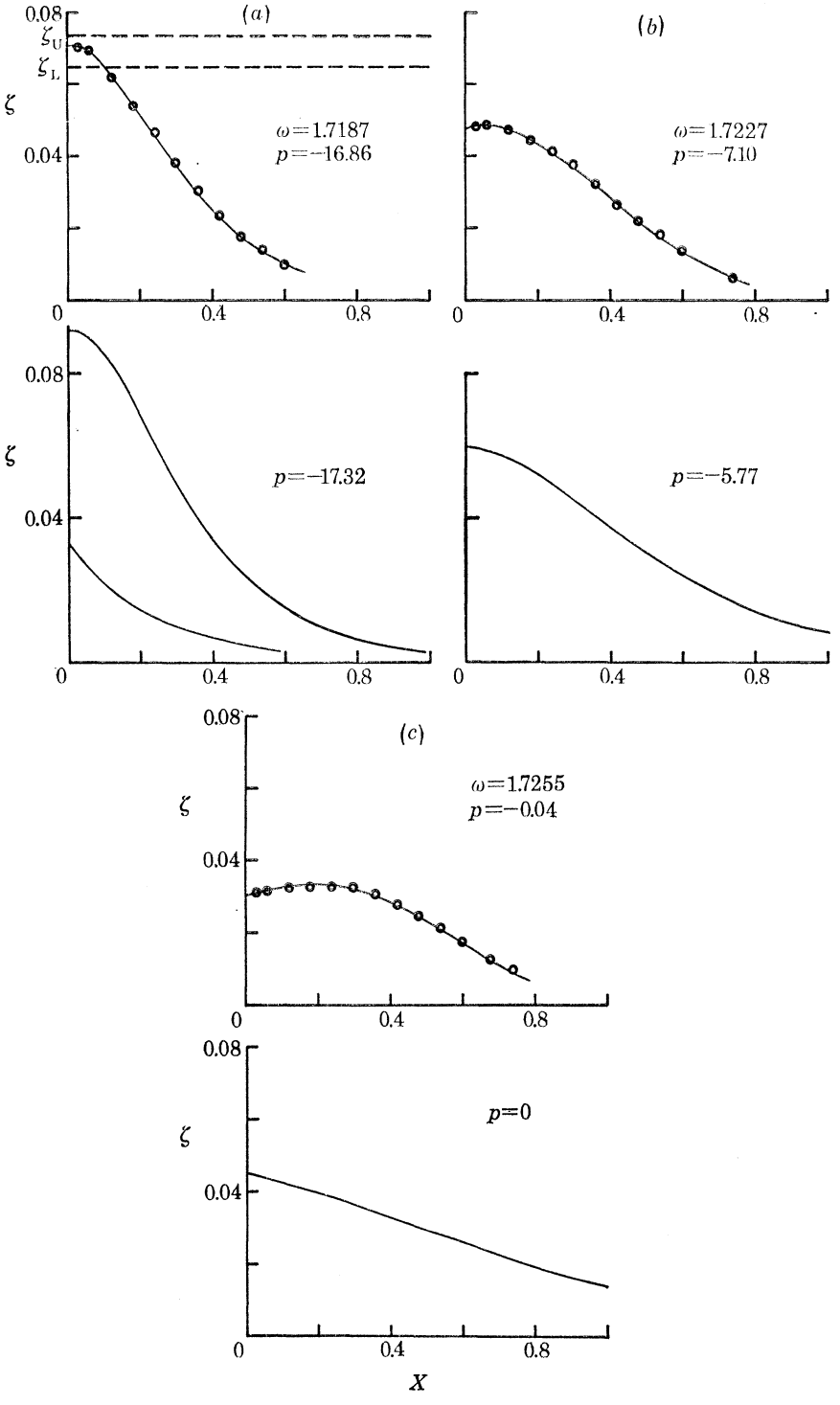

FIGURE 11. The amplitude response ζ along the channel for $\epsilon = 0.00783$ and for various values of ω (cf. figure 9). Note: the quantities ζ_L, ζ_U as calculated for the data (*a*), represent the range of the nonlinear inviscid solution which satisfies the empirical values of $\zeta(0)$, $\psi(0)$.

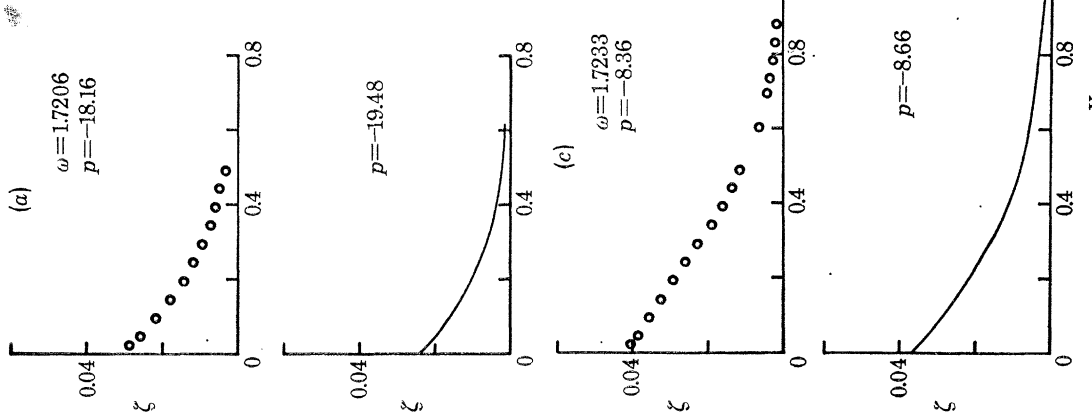

FIGURE 12. The amplitude response ζ along the channel for $\epsilon = 0.00527$ and for various values of ω (cf. figure 9).

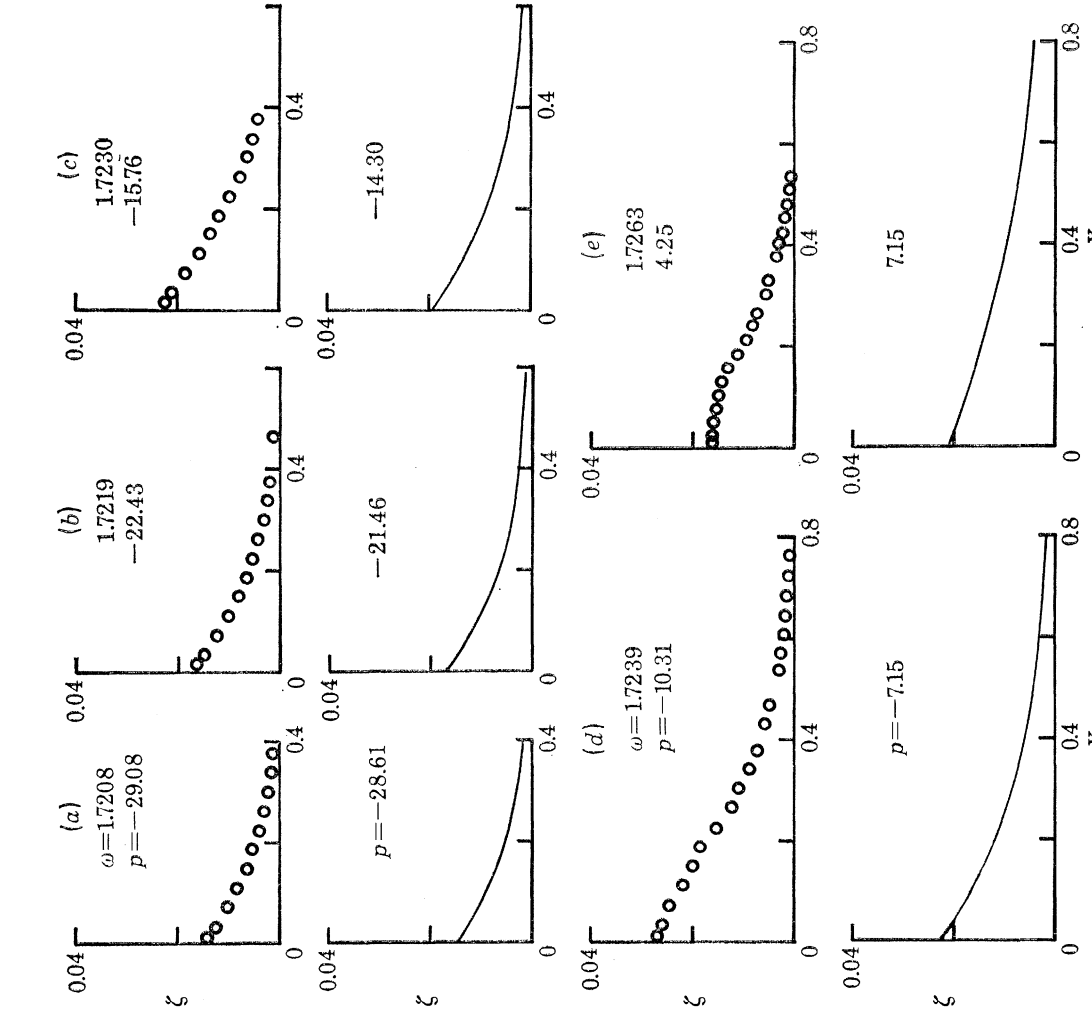

FIGURE 13. The amplitude response ζ along the channel for $\epsilon = 0.00316$ and for various values of ω (cf. figure 9).

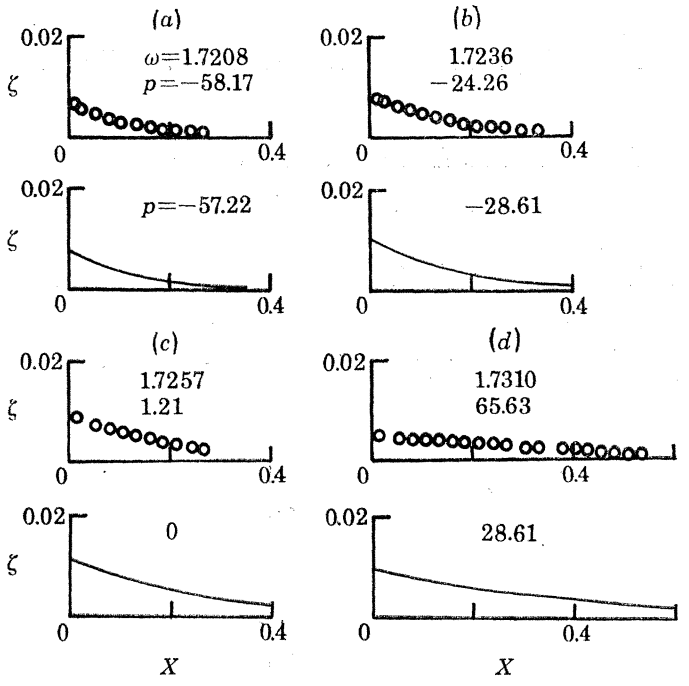

FIGURE 14. The amplitude response ζ along the channel for $\epsilon = 0.00158$ and for various values of ω (cf. figure 9).

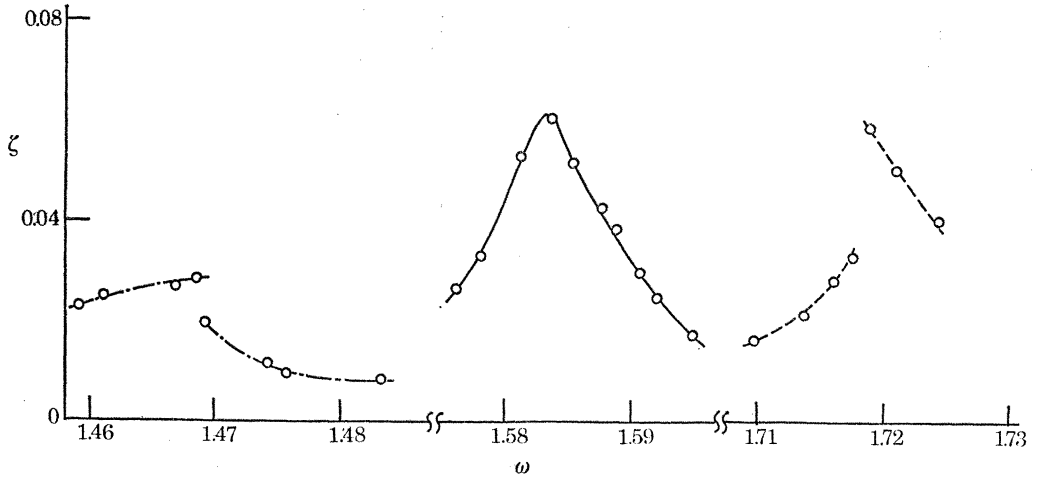

FIGURE 15. The response, as related to the frequency, for various values of the depth. — — —, $\beta = 0.556$; ——, $\beta = 0.341$; — · —, $\beta = 0.243$. The measurements were made at $\epsilon = 0.0067$ and $x = 0.645$.

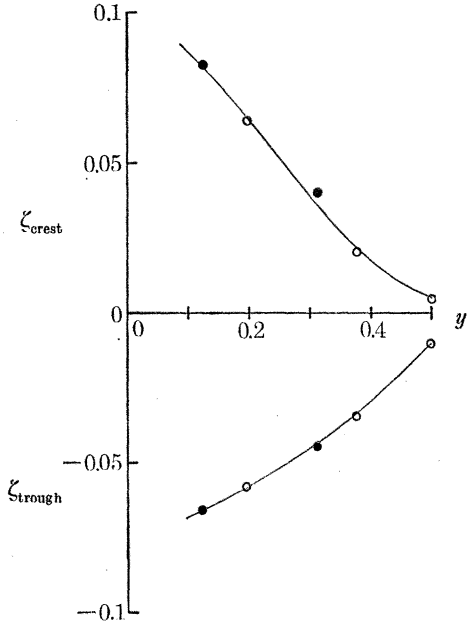

FIGURE 16. The wave crest and trough across the channel at $x = 0.653$, with $\epsilon = 0.0136$. ○, y is shown; ●, $1-y$ is plotted. $\beta = 0.555$.

Appendix A. A catalogue of failures

The first attempts at these experiments were made in a channel of width 30.4 cm and length 2.8 m. This was, in fact, the same channel as that used by Barnard & Pritchard (1972) for their study of the cross-wave instability, from which the present work evolved.

After a couple of false starts a set of measurements of the wave amplitude was finally completed and, as shown in figure A 1, the response at $X = 0.069$ appeared to agree fairly well with the inviscid solutions described in § 3.3. Accordingly, a draft manuscript on the project was prepared.

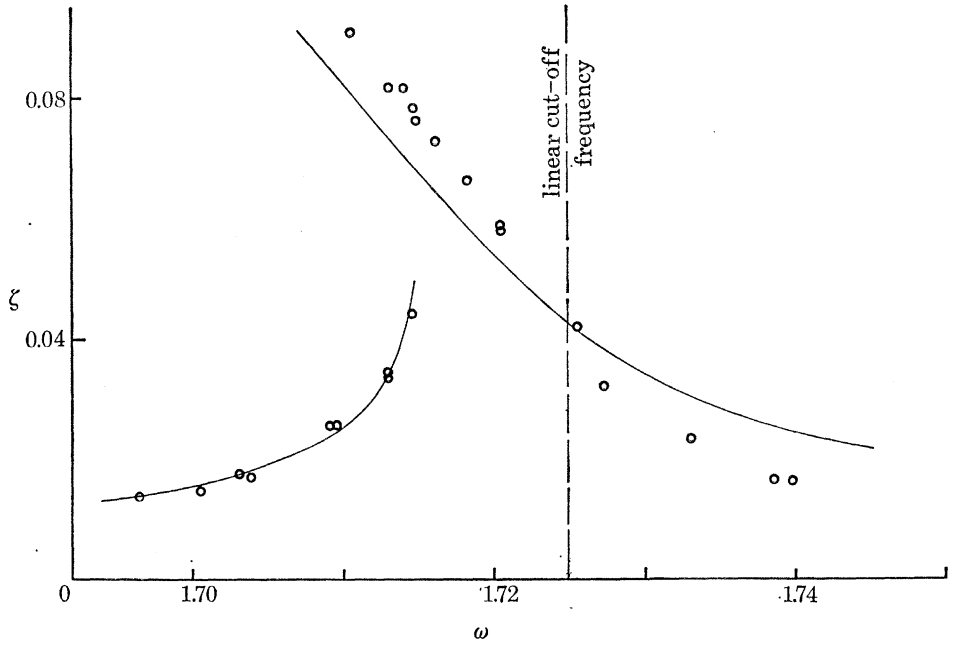

Figure A1. The amplitude response $\zeta(0.069)$ as related to the frequency ω, for some of the early experiments. The solutions are compared with the nonlinear inviscid theory (3.9, R_- branch, and 3.12). Note: an empirically determined frequency shift, of the kind described in relation to the data of figure 7, has been used here.

But we had some misgivings about the observed variation of ζ along the channel, which did not accord properly with the theory for the radiating-wave solution (3.12) (see figure A 2). The reason for this was not clear but there were a number of possible causes. For example, the channel was rather short, and it was felt that the presence of the beach may have been influencing the wave amplitudes: the toe of the beach was at $X = 0.46$ for the data shown in figure A 2. Alternatively, we thought that there might be yet another class of solutions to (3.4) which were in fact realized in the experiments. Thus, new experimental and theoretical attacks were made on the problem, and in the course of the new experiments we measured the phase of the waves. An analysis of these results indicated that, at frequencies a long way below cut off, the phase of the waves at the wavemaker was about $\frac{1}{4}\pi$ different from that predicted by linear theory. This discrepancy was most disconcerting, and a careful search suggested that a small amount of flexure in the paddle (about $\frac{1}{4}$ mm distortion at the maximum) could be the cause of the trouble. On stiffening the paddle the phase measurements then agreed with the linear theory at frequencies well below cut off, and so it was evident that we would need to repeat the complete set of measurements.

This new set of data yielded essentially the same wave amplitudes as those obtained in the earlier measurements. Moreover, experiments made with beaches of different slopes gave basically the same results. Therefore we were still left with a discrepancy between the measured values of the wave amplitude along the channel and the theoretical predictions from (3.12). In addition,

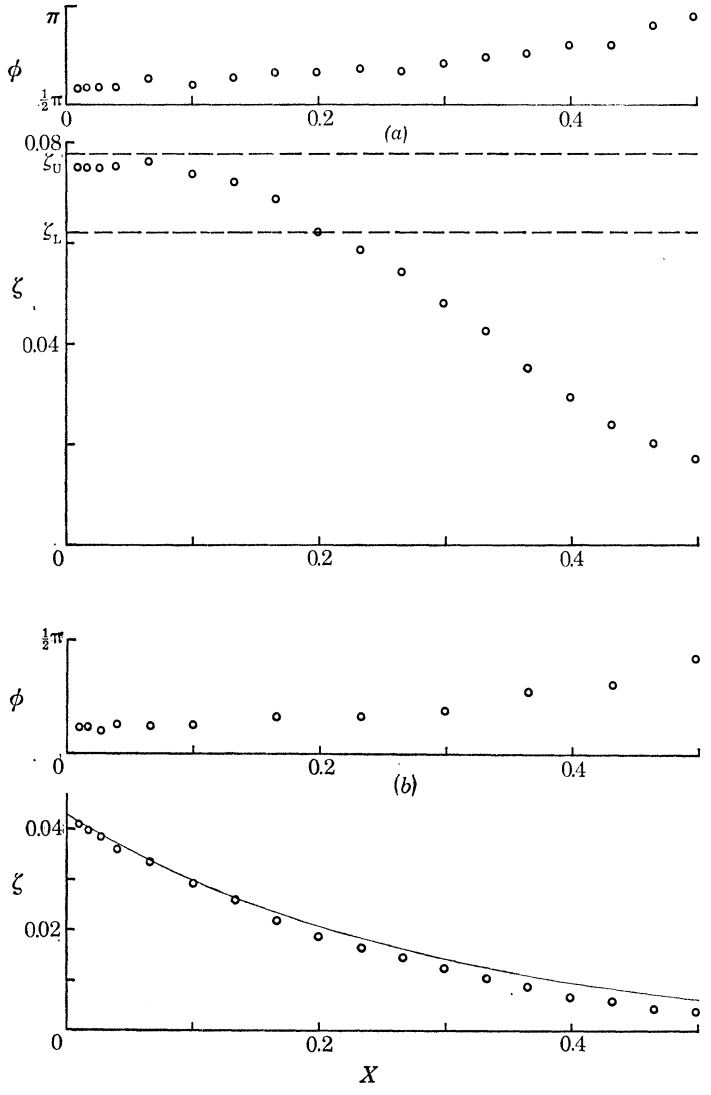

FIGURE A 2. The amplitude and phase measured along the channel for the experiments cited in figure A 1. (*a*) $\omega = 1.7143$; (*b*) $\omega = 1.7129$. In (*a*) is shown the range $[\zeta_L, \zeta_U]$ of the solution to the nonlinear inviscid model which satisfies the empirical values of $\zeta(0)$, $\psi(0)$. In (*b*) is shown the monotone decaying solution for ζ given by the nonlinear inviscid model.

progress on the theoretical side was being severely hampered by not knowing how to deduce the appropriate radiation condition. Accordingly, it was decided to test the applicability of the inviscid model-equation (3.4) by supplying the two unknown boundary conditions empirically, and then seeing how well the model could describe the wave amplitudes along the channel. In particular, we were interested to see if the inviscid model could, in any way possible, predict the large variation in $\zeta(X)$ indicated in figure A 2. For such a check we used the ideas outlined in § 3.3.3 to find the range of $\zeta(X)$ for given values of N and M^2. The actual values of N and M^2

relating to a given experiment were determined via (3.16), (3.15) and (3.7) from the measured values of $\zeta(0)$ (or equivalently $R(0)$ and $\psi(0)$). By determining N and M^2 from the empirical data in this way we will automatically be incorporating the standing-wave component in the tank resulting from the imperfect absorption at the beach. The outcome of such a test is shown in figure A 2*a* where the values of ζ predicted by (3.7) must lie in the interval $[\zeta_L, \zeta_U]$; but the empirical values of ζ fall well outside this range and so the conclusion is that the inviscid model is unable to describe the experimental results. Furthermore, checks were made to investigate the importance of errors in the measurements of $\zeta(0)$ and $\psi(0)$ on the theoretical range of ζ, and these indicated that the discrepancy could not be reconciled in such a way.

At about this time it was realized that the channel itself might be playing an important rôle in determining the structure of the motions because of variations in width and depth along the tank. For example, the width was found to vary by up to 2 mm from one end to the other and this is equivalent to changing the cut-off frequency γ by 0.002 s, which should be compared with a bandwidth of about 0.008 s for the nonlinear response. Thus the possibility existed that the non-uniformity of the channel was forcing the response into one of the 'decaying' solutions given by (3.9). Because of this weakness in our experimental method a new channel, of greater length, was constructed to the tolerances indicated above in §4. Accordingly, a new set of experiments were carried out (the results of these are described in the main part of the paper) and these confirmed our earlier conclusion that the inviscid model was not able to describe the experimental observations.

Appendix B. The magnitude of the dissipative effects

According to the theoretical discussion of § 2.3 the effects of dissipation are twofold, as described by the constants C_3 and C_4 of (2.21). The physical manifestation of the influence of C_3 is to introduce a (constant) frequency correction to the theoretical results: it is tantamount to a (usually small) modification of the cut-off frequency. This correction has been used for the comparison shown in figure 7, for which it was chosen to give the best agreement between the theoretical curves and the experimental results. However, as this correction is somewhat arbitrary we have used it only for figure 7 and for all other comparisons we have not made any such correction to the value of p.

The second (theoretical) influence of the dissipative effects occurs through the constant C_4, or the quantity q defined by (2.22). The numerical computations indicate that the value of the quantity q can have an important influence on the response observed in an experiment, as indicated by the results shown in figure 3. Thus, for the comparisons described in § 5, q was chosen in the following way.

The experimental results for $\epsilon = 0.01045$ and for $\epsilon = 0.00783$ both gave values for the phase $\phi(0)$ in excess of $\frac{1}{2}\pi$, which appears to be possible only when $\tilde{r} > 2.0$ (cf. figure 3*b*). On the other hand, at all other values of ϵ used in the experiments the phase $\phi(0)$ was less than $\frac{1}{2}\pi$, suggesting that $\tilde{r}$ should be less than 2.0 for such ϵ. The experimental results for the amplitude response indicated that two stable states were possible at certain frequencies when $\epsilon = 0.01045$ and $\epsilon = 0.00783$, but not when $\epsilon = 0.00527$. This suggests that $\tilde{r}$ should be less than 1.43 when $\epsilon = 0.00527$. Also, we wanted to choose a value of q so that the theoretical amplitude response corresponding to the smallest ϵ used in the experiments (where the nonlinear effects were negligible) agreed fairly well with the observations. A reasonable compromise appeared to be attained by choosing $\epsilon q = 0.046$ (though this was influenced a little by the fact that this choice was particu-

larly well suited to a number of the numerical computations that had already been made). This particular choice for ϵq predicts too large a response for the linear motions (at $\epsilon = 0.00158$), but larger values for ϵq, which would help correct this deficiency, give poor agreement with the data at the larger wavemaker amplitudes.

In the course of the early attempts at these experiments, as discussed in appendix A, some empirical estimates were made of ϵq using the method described in §§ 2.3, 3.2. These results suggested a value for ϵq of 0.085, a value which would give fairly good agreement between theory and experiment for the linear motions. However, such a value for ϵq would make $\tilde{r} = 1.13$ when $\epsilon = 0.01045$, which is much too small to give the kind of response observed empirically. We think the resolution of these difficulties probably lies in the quantity ϵq being amplitude dependent, and indeed, in retrospect, some of our 'direct' measurements of ϵq supported this hypothesis. A possible source of these difficulties is the wetting effect of the meniscus on the side walls of the channel.

References

Barnard, B. J. S. & Pritchard, W. G. 1972 Cross Waves. Part 2. Experiments. *J. Fluid Mech.* **55**, 245.

Cole, J. D. 1968 *Perturbation methods in applied mathematics*. Waltham, Mass.: Blaisdell.

Fultz, D. 1962 An experimental note on finite-amplitude standing gravity waves. *J. Fluid Mech.* **13**, 193.

Havelock, T. H. 1929 Forced surface waves on water. *Phil Mag.* **8**, 569.

Mahony, J. J. 1971 *Excitation of surface waves near to cut off frequency*. Fluid Mech. Res. Inst. Univ. of Essex rept. no. 7.

Nayfeh, A. H. 1973 *Perturbation methods*. New York: Wiley.

Ockendon, J. R. & Ockendon, H. 1973 Resonant surface waves. *J. Fluid Mech.* **59**, 397.

Tadjbakhsh, I. & Keller, J. B. 1960 Standing surface waves of finite amplitude. *J. Fluid Mech.* **8**, 442.

Ursell, F. 1952 Edge waves on a sloping beach. *Proc. R. Soc. Lond.* A **214**, 79.

PHILOSOPHICAL TRANSACTIONS OF THE ROYAL SOCIETY A MATHEMATICAL, PHYSICAL & ENGINEERING SCIENCES